

Cycle-calibrated magnetostratigraphy of middle Carnian from South China: Implications for Late Triassic time scale and termination of the Yangtze Platform



Yang Zhang ^{a,c}, Mingsong Li ^{a,b}, James G. Ogg ^{a,c,*}, Paul Montgomery ^d, Chunju Huang ^a, Zhong-Qiang Chen ^a, Zhiqiang Shi ^e, Paul Enos ^f, Daniel J. Lehrmann ^g

^a State Key Laboratory of Biogeology and Environmental Geology, School of Earth Sciences, China University of Geosciences, Wuhan 430074, Hubei, PR China

^b Department of Earth and Planetary Sciences, Johns Hopkins University, Baltimore, MD 21218, USA

^c Department of Earth, Atmospheric and Planetary Sciences, Purdue University, 550 Stadium Mall Drive, West Lafayette, IN 47907-2051, USA

^d Chevron Energy Technology Company, 1500 Louisiana Street, Houston, TX 77002, USA

^e Institute of Sedimentary Geology, Chengdu University of Technology, Chengdu 610059, Sichuan, PR China

^f Department of Geology, University of Kansas, Lawrence, KS 66045, USA

^g Department of Geoscience, Trinity University, San Antonio, TX 78212, USA

ARTICLE INFO

Article history:

Received 12 March 2015

Received in revised form 26 May 2015

Accepted 27 May 2015

Available online 9 June 2015

Keywords:

Triassic geomagnetic polarity time scale

Carnian cyclostratigraphy

405-kyr eccentricity tuning

Mid-Carnian Pluvial Event

ABSTRACT

Thick successions from the margins of the Triassic Yangtze Platform of the South China Block record a transition from carbonate-rich facies (Zhuganpo Formation and equivalents) to clastic-rich facies (Xiaowa Formation and equivalents) during the Carnian (early Late Triassic) that mark the final phase of termination of this long-lived platform. Cyclostratigraphy derived from spectral gamma-ray (SGR) intensity curves was combined with magnetostratigraphy of two sections in Guizhou Province (Wayao transect and its upward extension into the Geopark Wayao in Guanling county and the Laishike section in Zhenfeng county) and one location in Sichuan Province (Hanwang section). The cyclostratigraphy from all the Guizhou sections indicates a persistent suite of ca. 34 m, 9 m and 1.8 m cycles, which are consistent with the ratios of orbital-climate oscillations caused by long-eccentricity (405 kyr), short-eccentricity (~100 kyr) and precession (20 kyr). The magnetostratigraphy of all sections is consistent with the cyclicity and characteristic SGR features, thereby enabling a cycle-tuned magnetic polarity scale spanning ~2.4 myr. The main feature is a 1.3-myrr interval of reversed polarity containing brief normal-polarity subchrons, and this reversed-polarity chron appears to correspond to the significant reversed-polarity-dominated interval spanning the upper half of the *Trachyceras aenoides* through the lower half of the *Astrotrachyceras austriacum* ammonoid zones of the upper Julian (the lower substage of Carnian). This magnetostratigraphic correlation implies that the termination of the Yangtze Platform is coeval with the beginning of the mid-Carnian episode of climatic disruption in Europe, which is locally called the “Carnian Pluvial Event” or “Wet Intermezzo”, and with the temporary cessation of the platform carbonates in the Dolomites. The cycle-scaled magnetic-polarity time scale supports the “Short-Tuvalian/Long-Norian” age model of the Late Triassic in which the base of the cycle-tuned polarity pattern from the Newark Group of eastern North America is younger than the end of the Julian substage.

© 2015 Elsevier B.V. All rights reserved.

1. Introduction

During the middle of the Carnian Age (~230 Ma) of the early Late Triassic, there was a global disruption of Earth's climate-ocean-

biological system. This mid-Carnian episode, considered to be the most distinctive climate change within the Triassic (Preto et al., 2010), has been given various names depending upon the local characteristics, such as “Carnian Pluvial Event” in northern Europe, “Carnian Wet Intermezzo” in the Germanic Basin, “Reingraben turnover” in the Austrian Alps, or “Raibl Event” in the Italian Dolomites (e.g., Simms and Ruffell, 1989, 1990; Hornung and Brandner, 2005; Hornung et al., 2007a,b; Kozur and Bachmann, 2010; Dal Corso et al., 2012; Nakada et al., 2014; Ogg, 2015). This mid-Carnian episode was initially recognized within the Germanic Basin by an influx of fluvial to brackish-water sands into the arid facies of the Keuper and within the Alpine region by the termination of the prograding reefs of the earlier Carnian

* Corresponding author at: Department of Earth, Atmospheric and Planetary Sciences, Purdue University, 550 Stadium Mall Drive, West Lafayette, Indiana 47907-2051, USA.
Tel.: +1 765 494 8681.

E-mail addresses: zhangyang_wendy@163.com, zhan2214@purdue.edu (Y. Zhang), mli69@jhu.edu (M. Li), jogg@purdue.edu (J.G. Ogg), PMontgomery@chevron.com (P. Montgomery), huangcj@cug.edu.cn (C. Huang), zhong.qiang.chen@cug.edu.cn (Z.-Q. Chen), szqcdut@163.com (Z. Shi), enos@ku.edu (P. Enos), dlehrmann@trinity.edu (D.J. Lehrmann).

accompanied by a negative carbon-isotope excursion. These fluvial sands of the “Wet Intermezzo” in the Germanic Basin are correlated by conchostracean and megaspore assemblages to marine deposits of the upper part of the *Austrotrachyceras austriacum* ammonoid zone of the uppermost Julian substage (e.g., Kozur, 1975; Kozur and Bachmann, 2010) (Appendix Fig. A.2). [Note: The Julian substage is used here as the lower of a two-substage division of the Carnian stage following Krystyn (1974) and its common usage in many Triassic stratigraphy papers (e.g., majority of the reviews in Lucas (2010)), even though a distinct Cordevolian substage is recommended by Kozur (2003) and Kozur and Bachmann (2010) for the lowermost transitional interval spanning the *Daxatina canadiensis* and *Trachyceras aon* ammonoid zones that is characterized by co-occurrences of Ladinian and Carnian taxa.] The end to this “wet intermezzo” interval in the Germanic-Alpine region coincides with the substage boundary between Lower (Julian) and Upper (Tuvalian) substages of the Carnian. The trigger for

the onset of this mid-Carnian episode might be the eruption of the immense Wrangellia flood basalt province at ca. 230 Ma (e.g., Greene et al., 2010; Dal Corso et al., 2012), but uncertainties both in the age model for the Late Triassic biozones and in the stratigraphic age of the main eruptions of the Wrangellia volcanic province preclude a reliable correlation.

The Late Triassic currently lacks a high-precision integrated time scale. Indeed, estimates for the span of the Carnian stage range from ca. 16 myr to 8.5 myr, depending upon the choice between a “Long-Tuvalian” (hence, a short Norian) or a “Short-Tuvalian” (long Norian) option for its upper substage and upon other factors (e.g., reviews in Hounslow and Muttoni (2010); Lucas et al. (2012); Ogg, 2012; Ogg et al. (2014) (Fig. 1). A reference magnetic polarity time scale spanning 20 myr of the Late Triassic was developed from eccentricity-cycle-tuned scaling of the magnetostratigraphy from the fluvial-lacustrine Newark Supergroup of eastern North America (e.g., Kent and Olsen, 1999).

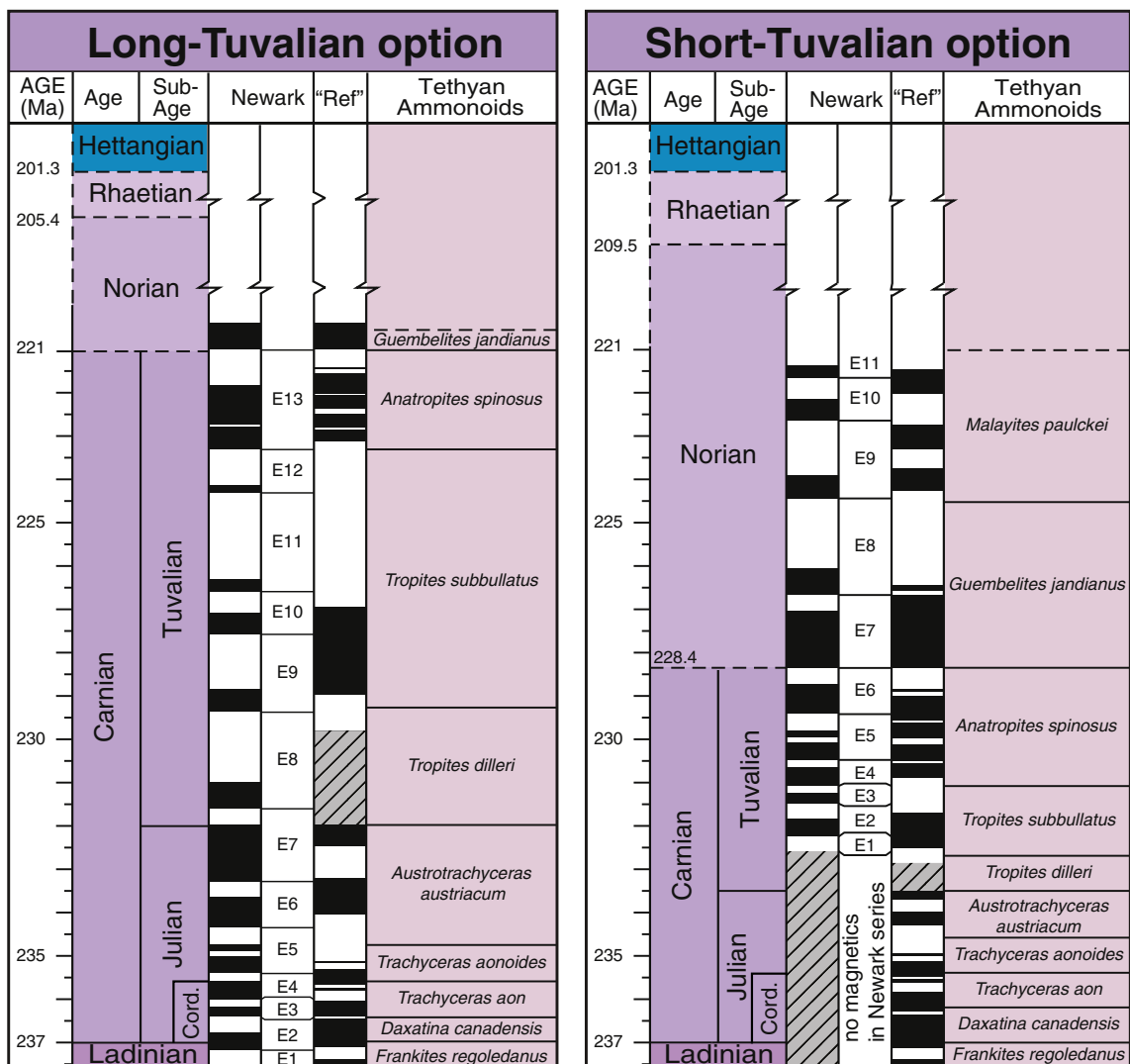


Fig. 1. Two end-member age models for Carnian and earliest Norian time scale (modified from Hounslow and Muttoni (2010); Ogg (2012)) for correlating the astronomical orbital-climate cycle-scaled magnetic polarity zones of the Newark group to the “reference” magnetic polarity scale (modified from Hounslow and Muttoni (2010)) derived from a synthesis of ammonoid- or conodont-dated outcrops. The broken and dashed lines are used to indicate a general view of the latest Triassic timescale. Left: A “Long-Tuvalian substage” option in which a relatively shorter Rhaetian is a hiatus in the Newark Basin, therefore the lowermost set of Newark polarity zone (E1–E13) is within the Carnian. Right: A “Short-Tuvalian substage” option with relatively longer Rhaetian present in the Newark Basin and a longer Norian implies that the Julian substage is older than the lowermost polarity zone in the Newark succession. In each option, the ages for the top of the Triassic (201.3 Ma) and base of the Carnian (237.0 Ma) are the same. See Hounslow and Muttoni (2010) and Ogg (2012, 2014) for details on the different Carnian–Norian–Rhaetian correlation possibilities. The dashed line indicates a working definition of the Carnian–Norian stage boundary; the International Commission on Stratigraphy has not decided on the GSSP placement. A two-substage division of the Carnian stage is used here; but the lowermost two ammonite zones are incorporated into a distinct Cordevolian substage by some stratigraphers (e.g., Kozur, 2003; Kozur and Bachmann, 2010).

Those Newark deposits reflect major variations in the seasonal strength of monsoonal precipitation as it was modulated by orbital-climate cycles at eccentricity and precession frequencies. Theoretically, as with the cycle-scaled polarity chronos that underpin the Cenozoic time scale, this Newark series should enable a precise Late Triassic time scale. However, calibrations of the Newark polarity scale to the independent magnetic stratigraphies derived from a partial assembly of many Late Triassic ammonoid- or conodont-zoned outcrops have many possible matches (e.g., Hounslow and Muttoni, 2010; and selected end-member options in Fig. 1). This ambiguity is also caused by the absence of cyclostratigraphy accompanying the magnetostratigraphy from those outcrop facies and by the lack of verified correlations of marine biozones to the succession of Newark terrestrial deposits. The lack of a verified Late Triassic age model and of a cycle-scaled bio-magnetostratigraphy scale hinders our ability to deduce the relative timing of events in different basins and to test the synchronicity and postulated causal factors for this proposed global warming pulse.

Our combined magnetostratigraphy and cyclostratigraphy study of expanded sections of middle Carnian shelfal to basinal facies near the margins of the Yangtze Platform has three main objectives. (1) Compile an integrated scale of magnetostratigraphy, spectral-gamma-ray intensity, biostratigraphy and cyclostratigraphy to test whether the termination of the Yangtze Platform shallow-water carbonates is approximately synchronous between its southern (Guizhou) and northwest (Sichuan) margins. (2) Correlate to outcrop-based magnetostratigraphies from fossiliferous European sections to determine if final phase of termination of the Yangtze Platform carbonates as marked by the influx of

clastic-rich facies was during the latest Julian and therefore coeval with the "Wet Intermezzo" or "Carnian Pluvial Event". (3) Apply the cycle-scaling of the durations of major polarity zones through the middle Carnian of South China to determine which portions of the pattern, if any, have corresponding cycle-scaled polarity chronos in the Newark geomagnetic scale, therefore placing constraints on the entire Late Triassic time scale.

2. Geologic setting of Yangtze Platform sections

During the Triassic, the South China Block was situated between the Panthalassa Ocean to the east and the seas and the seaways of the Paleo- and Meso-Tethys to the west and the south (Fig. 2). The Yangtze Platform of South China, considered to be one of the Earth's largest regions of shallow-water deposition, covered most of the present Guizhou Province and parts of neighboring Sichuan, Yunnan, Guangxi, and Hunan provinces. Thick successions of shallow-water carbonates span much of the late Proterozoic through the mid-Triassic. This Yangtze Platform and many other Triassic carbonate platforms were terminated in the Carnian, but unlike the Dolomites and Alpine regions, carbonate deposition on this Yangtze Platform never resumed and its overlying Norian deposits are typically braided river systems emptying into coastal swamps (e.g., Lehrmann et al., 2014; Minzoni et al., 2015). A detailed synthesis of the Triassic facies history is compiled in Feng et al. (1997) and in Enos et al. (2006).

The Carnian sediments in the southern and western portions of the Yangtze Platform and its adjacent basins have variable facies

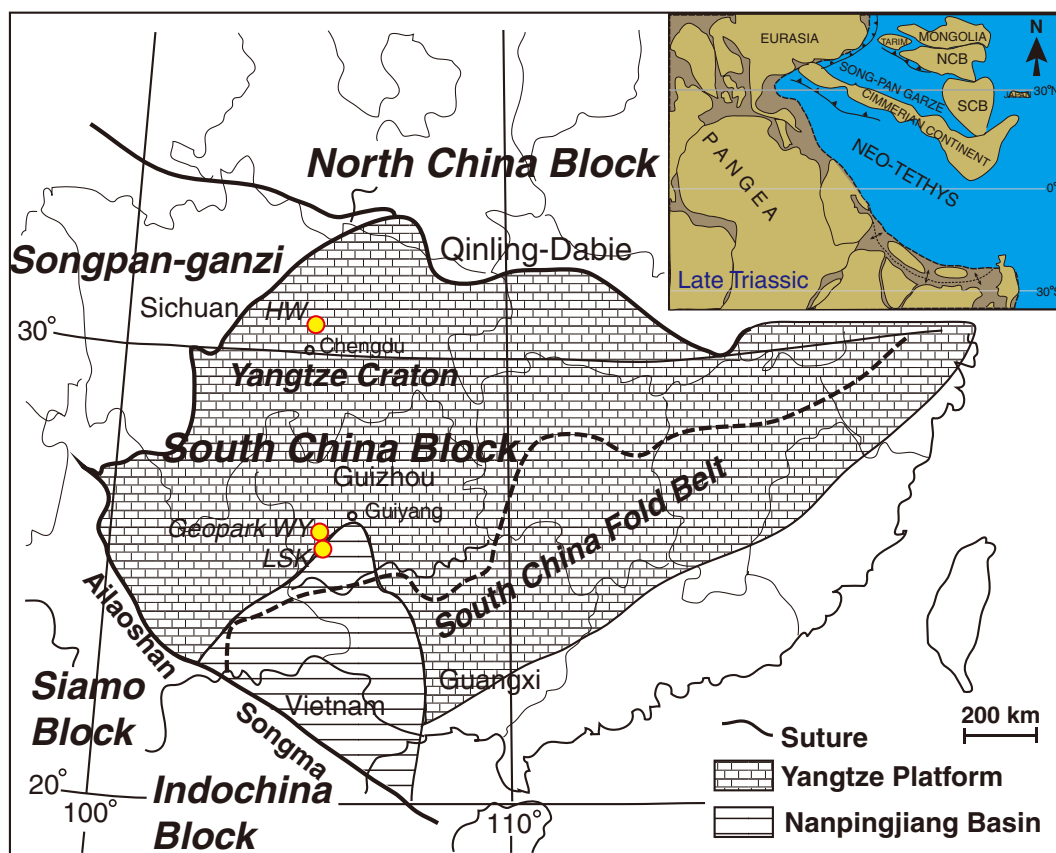


Fig. 2. Locations of the three sections (shown as yellow dots) in South China on generalized tectonic map modified from Lehrmann et al. (2005) and Wang et al. (2008). WY: Geopark Wayao section in Guanling county, Guizhou; LSK: Laishike section in Zhenfeng county, Guizhou; HW: Hanwang section in Mianzhu county, Sichuan. The Yangtze Platform includes the Yangtze Craton and South China Fold Belt of the South China Block. Inset in upper right is a Late Triassic plate reconstruction of the South China Block (SCB) at its initial collision with the North China Block (NCB) (modified from Besse et al. (1998); Golonka (2007)).

superimposed on the common deepening trend, therefore different formation names are used in different locations (e.g. reviewed in Gu and Liu (1997); Dong et al. (1997); Enos et al. (2006)). The compilation of paleofacies maps to unravel their relationships is partly hindered by apparent disagreements in assigning precise biostratigraphic ages between the conodont ranges and the ammonoid assemblages within the same stratigraphic levels in some formations.

The South China Block progressively drifted north during the Triassic, and was located c. 30°N during the Late Triassic (e.g., reconstructions in Scotese (2001)). After the mid-Triassic, the South China Block sutured with the North China Block to the north and with the Indochina and Siamo blocks to the south and west (e.g., reviews and paleotectonic reconstructions in Wang et al. (2000, 2008); Scotese (2001)).

We sampled two representative sections in Guizhou province near the Yangtze Platform southern margin (Geopark Wayao = WY, Laishike = LSK), and one typical section of its western margin in the present Sichuan province (Hanwang = HW) (Fig. 2 and Appendix Fig. A.1). The locations and stratigraphy of each section are detailed in the Appendices.

3. Magnetostratigraphy and cyclostratigraphy results

The magnetostratigraphy and cyclostratigraphy of the composite Wayao sections are detailed here. The appendices contain details of

the magnetostatigraphy and cyclostratigraphy for the Laishike and Hanwang sections, examples of demagnetization diagrams, enlarged vertical scale stratigraphic figures for the Wayao sections, and data tables.

3.1. Composite Wayao (WY) section – magnetostratigraphy

The magnetic directions in the laminated dark-gray calcareous claystones of the lower Xiaowa Formation display an initial clustering centered near present field at initial demagnetization at 5 mT and 150 °C, and then a progressive drift toward opposing directions that is most pronounced for the 300–375 °C interval (Appendix Fig. D.1 WY). The lithology begins to develop a reddish color upon heating above 325 °C, but this onset of thermal alternation did not appear to significantly affect the magnetic-vector directions or the magnetic susceptibility. The remnant magnetization of most samples became too weak to reliably measure or began to display anomalous shifts in directions with an increase in intensity that was often accompanied by an increase in susceptibility at or above 400 °C. Montgomery et al. (2003), and in Minzoni et al. (2015) suggested that this might be formation of new magnetic minerals from the oxidation of iron sulfides, but dehydration of iron-rich clays (e.g., goethite) may also play a role. The characteristic directions of magnetization were usually computed using the 300–375 °C range for each sample. Three-axis IRM studies (Minzoni et al., 2015) indicated unblocking temperatures of ca. 300° for “soft” (0.1 T)

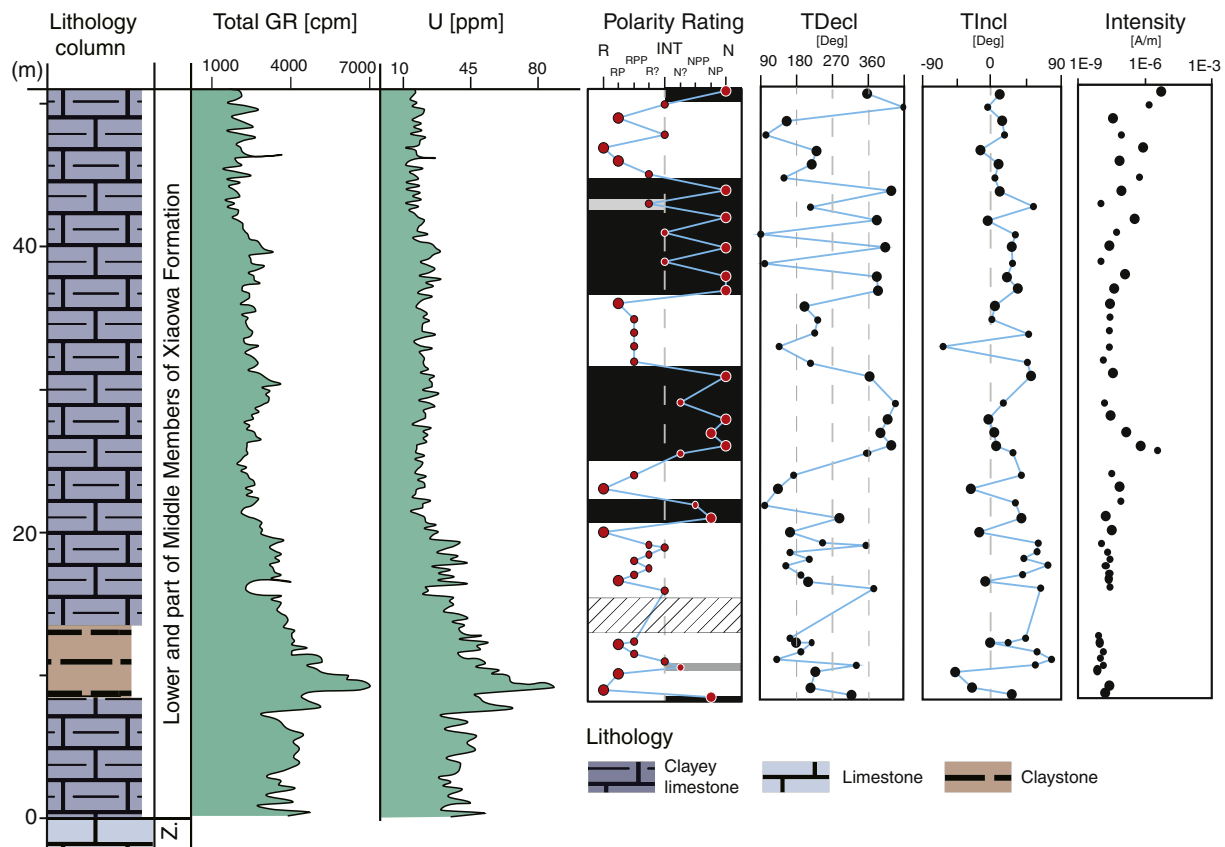


Fig. 3. Magnetostratigraphy of the Lower and part of Middle members of the Xiaowa Formation at the Geopark Wayao (WY) suite of quarries with the total (gamma ray; GR) and Uranium (U)-spectra gamma-ray intensity. The major peak of the GR and U corresponds to the onset of an organic-rich clay interval, which is the “zero” level for precise correlation with previous (Montgomery et al. (2003), and in Minzoni et al. (2015)) Wayao magnetostratigraphy section. Polarity rating (N to INT to R as explained in Appendix B) has superimposed black bars for normal-polarity zones, white bars for reversed polarity, gray bars for clusters of indeterminate and intermediate (INT) vectors, and diagonal-line shading for sample gaps. Declination-inclination-intensity values are for the vectors computed by least-squares from the characteristic magnetization steps in stratigraphic (bedding tilt-corrected) coordinates. Larger dots indicate the N/NP- and R/RP-rated vectors used in the computation of mean directions.

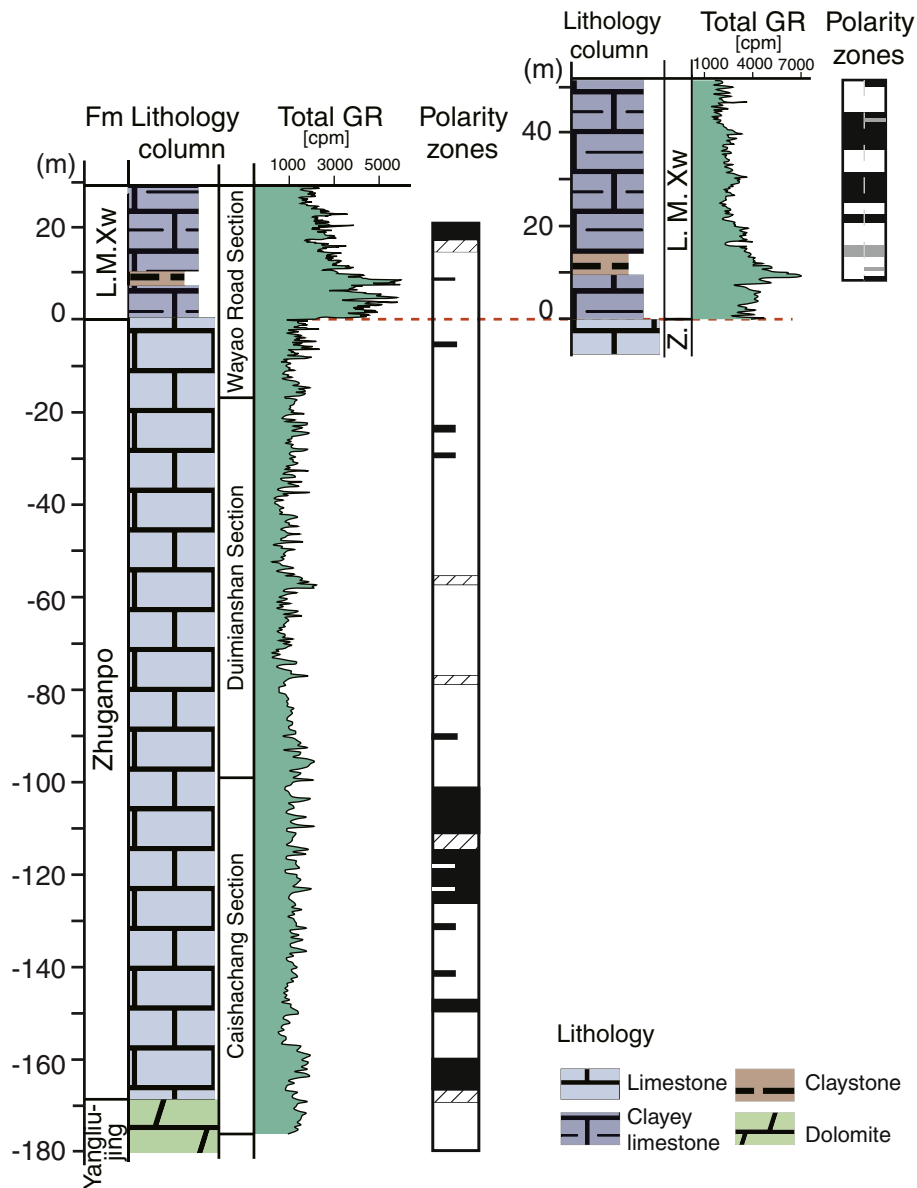


Fig. 4. The magnetostratigraphy of the Wayao Transect (modified from Montgomery et al. (2003), and in Minzoni et al. (2015)) (left) and its upward extension from the Geopark Wayao section (Fig. 3) (right). The “0” level is the contact between the Zhuganpo and Xiaowa formations, and the gamma-ray logging spanned beyond the magnetostratigraphic sampling in both sections. The composite Wayao gamma-ray intensity curve is from the Caishachang, Duimianshan and Wayao Road sections adjacent to the earlier magnetostratigraphy traverse. Expanded stratigraphic sections are in the Appendix.

and “medium” (0.4 T) IRM and ca. 580 °C for “hard” (1.2 T) IRM for both the laminated dark-gray clay-rich lithology and for the underlying gray limestones. The combination of the lithology colors, unblocking temperatures and IRM studies suggest that there is a magnetization carried by goethite in the clay components that is removed at ca. 250 °C, followed by a dominance of magnetization carried by magnetite for the characteristic directions in the 300–375 °C range, with a very minor component carried by hematite. Pyrrhotite minerals within the iron-sulfide components could contribute a magnetic component, but that most of the characteristic directions obtained in the 325–400 °C range were dominated by a primary magnetite signal (e.g., Minzoni et al., 2015).

Even though there is a distinct drift in magnetization vectors toward opposing polarity directions through the 200–400 °C interval, only a small fraction (20%) of the laminated clay-rich Xiaowa

Formation samples attained an endpoint direction that was stable with decreasing intensity upon additional heating, which are the criteria for the N/R quality rating. This was particularly true for the majority that progressively drifted toward the reversed hemisphere, where only 3 samples attained a stable ‘R’ direction and only 6 were classified as ‘RP’. However, even after giving ‘P’-rated directions half weight and omitting the preponderance of ‘PP’- and ‘?’-rated, the mean directions of the few filtered samples are antipodal when considering the confidence levels: Normal-polarity clusters at 32° declination, 18° inclination (17° alpha-95) and Reversed-polarity clusters at 194° declination, −14° inclination (with a high 32° alpha-95, as explained above) (Appendix Table D.1; Fig. D.1). The log-mean vector intensity for the mean N/NP-rated direction is over twice as strong as for the mean R/RP-rated direction, which may reflect a combined effect from the facies change from the low magnetic intensities of the

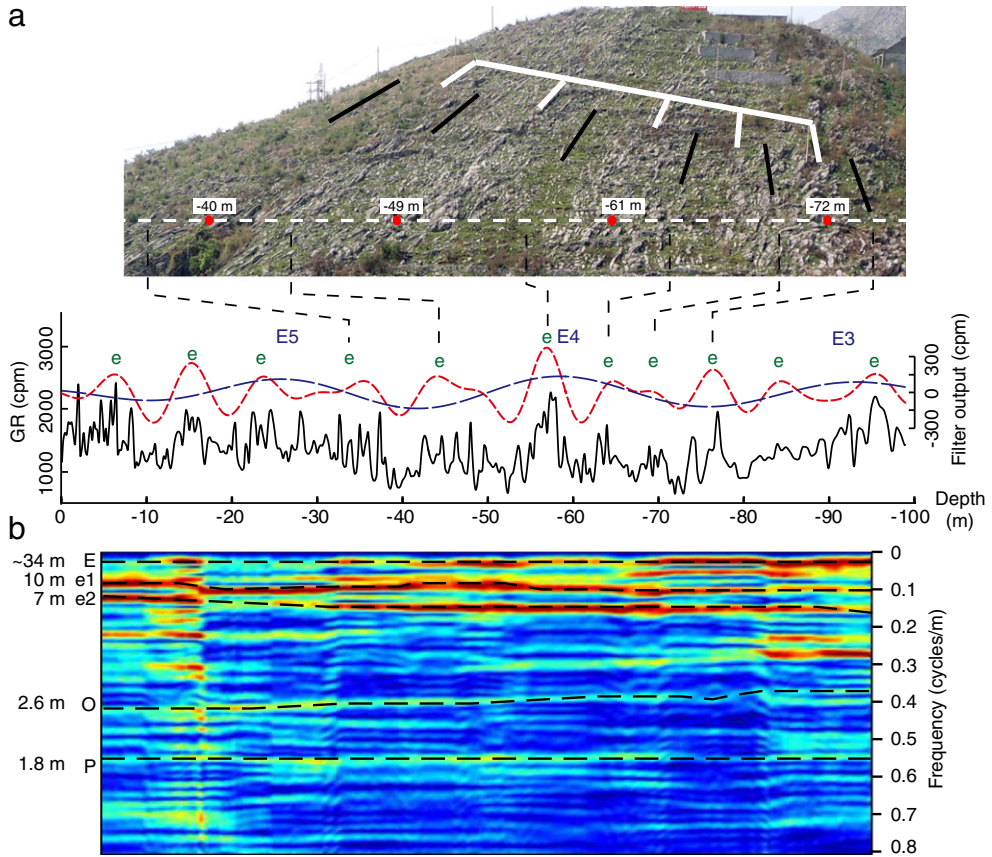


Fig. 5. (a) Photo and GR signal of the middle part of the Zhuganpo Formation at the Wayao Transect. Relatively clay-rich intervals are less resistant to weathering (indicated by black lines and dashed continuations) and correspond to relative peaks of higher values in the smoothed GR signal. Limestone-rich intervals (white lines and corresponding meter-labels at red dots on white-dashed transect) are relative troughs in the GR signal. Detrended and band-passed GR signal (Gauss filter, passband: 0.029 ± 0.01 and 0.11 ± 0.03 cycles/m, respectively; Fig. 6) indicates a ~34 m envelope (blue with blue labels) on ~9 m cycles (red with green labels at clay-rich peaks). The peaks of the ~9 m cycles are interpreted as ~100-kyr short-eccentricity maxima modulated by the 405-kyr long-eccentricity cycles. (b) Evolutionary Fast Fourier Transform (FFT) spectrum using a 50 m sliding window. The black dashed lines correspond to the significant cycles which relate to possible astronomical parameters.

reversed-polarity-dominated black claystones of the basal portion and from perhaps a residual north-directed overprint on both sets. The mean direction of the combined suite indicates a paleolatitude of 9°N , but with an 8° uncertainty; and this clay-rich facies probably has a significant inclination shallowing caused by post-depositional compaction flattening.

The stratigraphic clustering of the interpreted characteristic directions and polarity ratings of our extension upward into the middle Xiaowa Formation displays two significant normal-polarity zones within a predominantly reversed-polarity succession (Fig. 3). The reversed-dominated lower half of the 2014 section overlaps and partly extends upward the major reversed-polarity zone of Montgomery et al. (2003), and in Minzoni et al. (2015) (Fig. 4).

The interpretation that these polarity zones represent Carnian magnetic-polarity chronos is supported by several lines of evidence, which is partly detailed in Minzoni et al. (2015): (1) the mean directions, paleolatitudes, and post-magnetization rotations for the Wayao suites are consistent with those of other Middle and Late Triassic paleomagnetic studies in the South China Block (e.g., synthesis by Enkin et al. (1992); see Appendix Table D.1); (2) the clusters of normal- and reversed-polarity directions pass both a reversal test and a fold test for the Zhuganpo Formation; and (3) the main characteristics of the polarity pattern are reproduced in coeval strata within the Wayao suite and at Laishike, as described below.

3.2. Composite Wayao (WY) section – cyclostratigraphy

The limestone beds of the Zhuganpo Formation displays patterns of variable bed thicknesses and changing clay content within the limestones as reflected in relative weathering resistance. These factors influence the natural gamma-ray signal with higher intensities indicating higher average clay contents (Figs. 5 and 6).

The power spectra of the GR series from the Zhuganpo limestones show a suite of significant cycles above 95% confidence levels at ~34 m and ~9 m (split into 7 m and 10 m; Fig. 5b) and of short-wavelength peaks at 2.6 m and 1.8 m (Fig. 6b). Band-pass filtering of the GR signal and visual examination of the medium-wavelength GR peaks in the original data indicate that the range of "10 m" and "7 m" peaks are partly an artifact of semi-consistent thickening and thinning of these intermediate cycles under the ~34-m envelope and partly caused by a slight thickening of these cycles in the upper 50 m of the formation. The average intermediate peak is ~8.5 m. Therefore, the ratio of the long-wavelength (~34 m) to this intermediate-wavelength cycles is ~4.0, which is the same ratio (~4:1) of long-period eccentricity (405 kyr) to the average short-term eccentricity (100 kyr) cycles. Extending upward the interpretation that the main peaks in GR at ca. 9-m intervals correspond to the 100-kyr short-eccentricity cycles with an implicit assumption that the onset of the clay-rich facies of the lower Xiaowa Formation did not cause a sudden discontinuity in

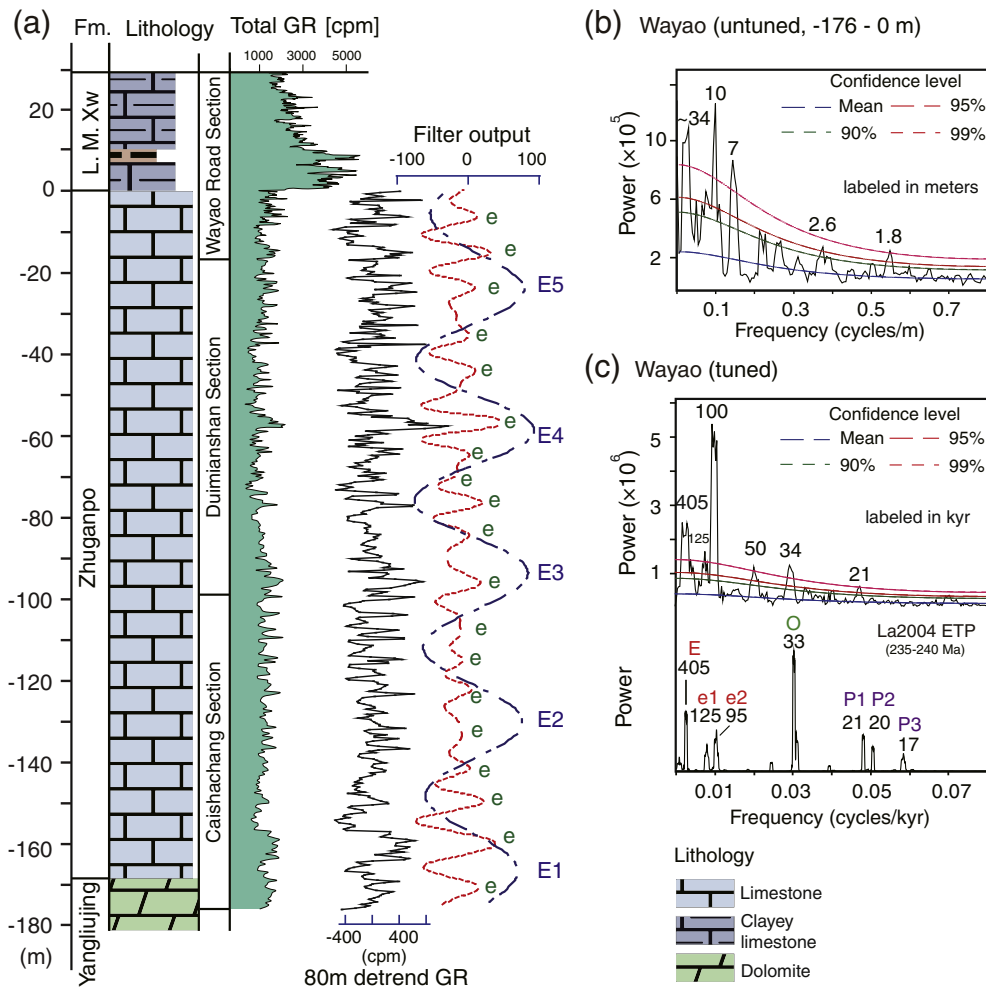


Fig. 6. Cyclostratigraphy of the Wayao section. (a) The composite Wayao GR with filtered ~34 m (blue) and ~9 m cycles (red) (Gauss filter, passband: 0.029 ± 0.01 and 0.11 ± 0.05 cycles/m, respectively). (b) 2π multi-taper method (MTM) power spectrum of the Zhuganpo Fm. from -176 m to 0 m, after removing the 80-m lowess trend. (c) 2π MTM power spectrum of the tuned Zhuganpo Formation GR time series (upper panel) after removing a 1-myrr lowess (a locally weighted scatterplot smoothing method) trend, and assigning 100 kyr to the peak of each ~9-m filtered cycle; the lower scale is the La2004 model from 235 to 240 Ma (Laskar et al., 2004) showing predicted astronomical-cycle frequencies (E: 405 kyr eccentricity; e: ~100 kyr eccentricity; O: obliquity; P: precession) for early Carnian age. A robust red-noise model is calculated with linear fitting and a 20% median smoothing window.

sedimentation rates, then a set of 100-kyr levels were assigned to the most pronounced GR peaks in this Lower Member (Figs. 6a, 7a). There are possibilities that, relative to the underlying Zhuganpo Formation, the clay-rich lower Xiaowa Formation has a higher accumulation rate from the clay influx or alternatively that it is more condensed from the cessation of micritic carbonate influx, but our interpretation is that the GR peaks reflect the same orbital-climate-facies signal. The identification of short- and long-eccentricity cycles within these formations implies that the associated geomagnetic polarity scale spans approximately 2.4 myr, and allows durations to be assigned to each major polarity zone.

The Average Spectral Misfit (ASM) method (Meyers and Sageman, 2007) provides a test for rejecting the null hypothesis (no orbital signal) and objective estimation of the optimal sedimentation rate for a stratigraphic interval that was influenced by astronomical forcing. Applying ASM to the WY section implies that the null hypothesis (H_0 , no orbital forcing) could be rejected and that the optimal accumulation rate is ~10.0 cm/kyr. Details are in Appendix E.

Similar oscillating accumulation rates affected the short-wavelength cycles, and the ratio of ~1.8 m to the ~8.5 m intermediate cycle is the same 1:5 ratio as the precession periodicity (~20 kyr) to the short-eccentricity (~100 kyr). An initial 405-kyr tuning trial followed by a

higher-resolution 100-kyr tuning of the ca. 8.5-m-spaced-peaks was applied to the filtered series through the Zhuganpo Formation (Fig. 6c) followed by spectral analysis. This dual-tuning (405-kyr and then 100-kyr) is similar to the procedure used by Huang et al. (2010) for resolving high-resolution durations of ammonoid ones in the late Jurassic Kimmeridge Clay. Tuning assignments were partly guided by comparing windows in the evolutive spectra to identify any irregular discontinuities or shifts in spectral bands. The final 100-kyr tuned spectra indicates that the main short-wavelength peak (the only one above 95% confidence) corresponds to 20 kyr, which is the same as the predicted dominant precession cycles (20.7 and 19.7 kyr) for the Carnian under the La2004 astronomical solution (Laskar et al., 2004) (Fig. 6c).

4. Discussion

4.1. Composite cycle-tuned geomagnetic polarity time scale for middle Carnian

The magnetostratigraphy of the two adjacent sections at Wayao is lithostratigraphically correlated from the facies change at the base of the Xiaowa Formation and the following distinctive peak in GR at the base of the black-shale interval at the ~10 m level (Fig. 4). Therefore,

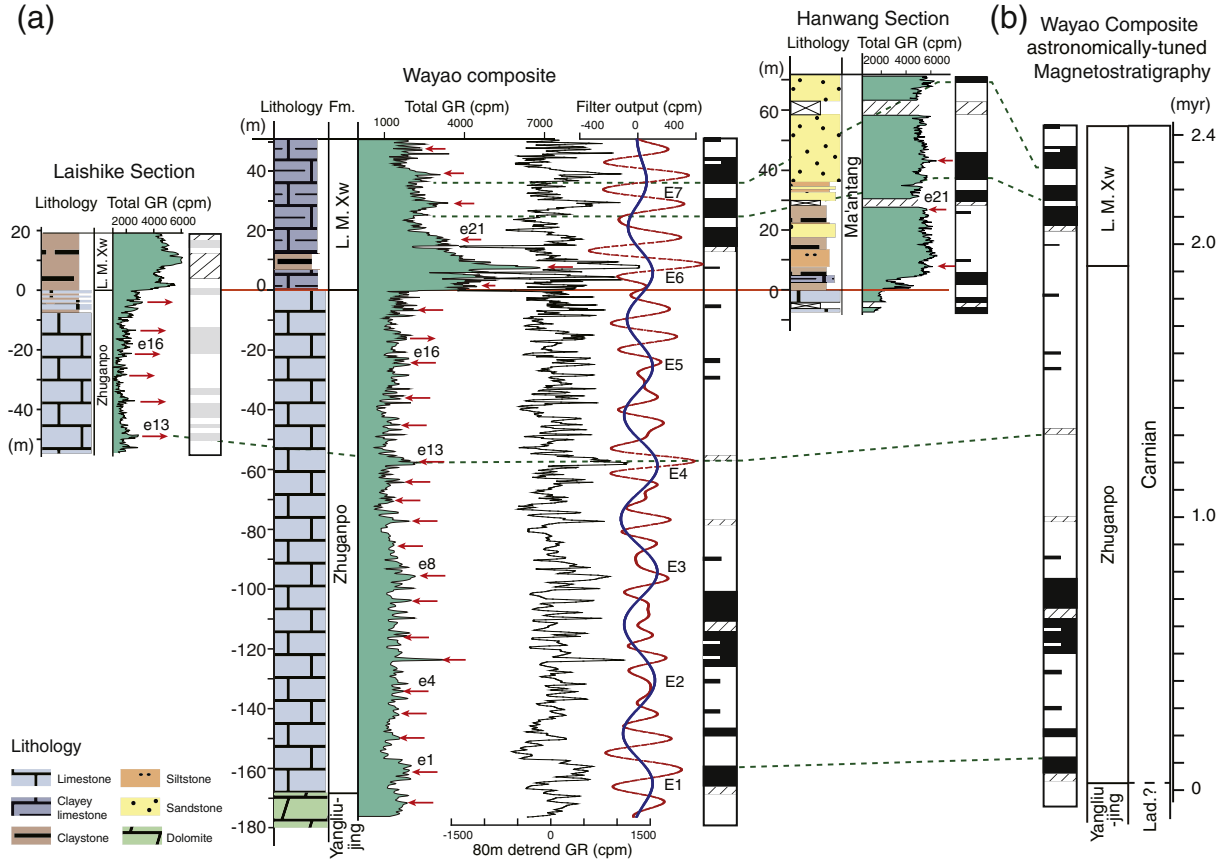


Fig. 7. (a) Correlation of the Laishike section, the Wayao composite (modified from Minzoni et al. (2015); and with upward continuation with the Geopark Wayao section), and the Hanwang section according to magnetostratigraphy (dashed green lines) is guided by cyclostratigraphy. See Fig. 6 for explanation of Wayao composite curves. Expanded stratigraphic columns of the Laishike and Hanwang sections are in the Appendix. Red arrows (with numbers) are interpreted 100-kyr short-eccentricity peaks. (b) The composite astronomically-tuned floating timescale for this geomagnetic polarity pattern is based on the 100-kyr cycle tuning of the composite Wayao sections and supported by partial duplication of the cyclostratigraphy in the Laishike section.

the capping normal-polarity zone of the Wayao transect (Montgomery et al. (2003), and in Minzoni et al. (2015)) corresponds to the lowest normal-polarity band in the Geopark Wayao set. The cyclostratigraphy of the GR curve from the limestone succession of Wayao indicates that there are ca. 9-m-wavelength cycles (100-kyr eccentricity) with relative peaks in clay content (higher GR) within an envelope of ca. 34-m cycles (405-kyr eccentricity) (see Section 3.2). If the rate of accumulation continued into the lower Xiaowa Formation of the Geopark Wayao section, then the overlying suite of 5 relative peaks in GR (clay-enrichment) with a similar ~9-m spacing is a continuation of these 100-kyr climatic cycles.

The cyclostratigraphy results from Wayao match the interpreted Milankovitch signals within the mid-Carnian carbonate-ramp facies (Dürrenstein and Raibl formations) in the Dolomites of northern Italy (Preto and Hinnov, 2003). Power spectra of that tuned rank-series revealed cycles of 400-kyr long-eccentricity, a pair of 125-kyr and 95-kyr short-eccentricity and a pair of 21.9-kyr and 17.8-kyr precession periods, which are similar with our power spectra for a partially coeval age interval in southern China.

The Zhuganpo through lowermost Xiaowa formations at Laishike duplicate the same reversed-polarity interval as at Wayao. The clusters of 'N?' levels at Laishike are not reliable features, therefore the potential brief normal-polarity horizons within this major reversed-polarity zone at Wayao are not yet verified. The cyclostratigraphy from spectral analysis of the Laishike section displays the same ratio of ~10 and 1.9 m cycles within an envelope of ~34 m as the Wayao section

(Fig. E.3). This similarity in the cyclostratigraphy wavelengths, the GR signature of the basal Xiaowa Formation and the common reversed-polarity dominance allow a proposed correlation of the ca. 9-m '100-kyr' peaks in GR between Laishike and Wayao (red arrows in Fig. 7). Unfortunately, deep weathering and agricultural fields at Laishike precluded duplication of the overlying dual-polarity pattern of the Geopark Wayao continuation, but future magnetostratigraphy work at Laishike might be able to obtain a signature polarity pattern from the underlying limestones to verify the mixed polarity of the lower Zhuganpo Formation at Wayao.

Correlation using magnetostratigraphy and GR-trends to the Hanwang section of Sichuan is speculative, because of (a) the interpretation of a hiatus of uncertain duration at the sudden contact of thin black shale onto the oolitic beds (our '0' level) in contrast to a compact but gradual transition to laminated clay-rich facies at the Wayao and Laishike sections, and (b) the pronounced increase in silt and sand sedimentation rates in the higher levels of the Hanwang section compared to a continuation of a more quiet-water setting for the laminated clay-rich facies at Wayao and Laishike. Therefore, the suggested correlation of the magnetostratigraphy (dashed green lines in Fig. 7a) is based on three assumptions: (1) a hiatus at the abrupt onset of the black shale at Hanwang has removed the equivalence of the reversed-polarity limestones of the upper Zhuganpo, therefore the normal-polarity of the underlying oolitic limestone at Hanwang has an uncertain equivalence in the lower part of the Wayao succession; (2) the reversed-polarity-dominated, clay-rich, high-GR interval of the lower ca. 30 m of Hanwang

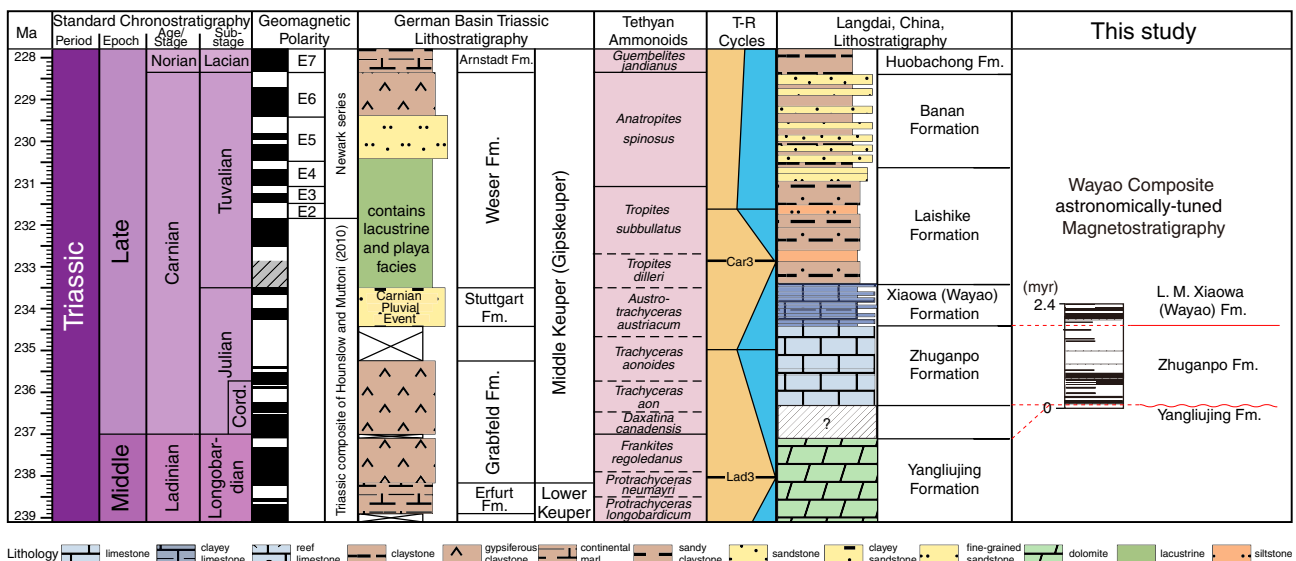


Fig. 8. Proposed correlation of the 2.4-my interval of cycle-tuned magnetostratigraphy of the Wayao composite (Fig. 7b) to the geomagnetic polarity patterns of Tethyan ammonoid zones (Hounslow and Muttoni, 2010) in a modified version of the "Short-Tuvalian" age model option (Fig. 1; Appendix Fig. A.2) for the Carnian. If the age limits of the Julian substage are maintained, then the correlation of the 1.3-my reversed-polarity zone in the Zhuganpo Formation to the main reversed-polarity zone in the Julian implies a relatively longer duration to its upper two ammonoid zones relative to the lower two zones; and this scaling is shown here to adjust the other stratigraphic scales. The dashed red lines on the right are the boundaries of the formations. The magnetostratigraphy correlation implies that the base of the clay-rich Lower Member of the Xiaowa Formation begins in the middle of the *A. austriacum* ammonoid zone and is coeval with the "Carnian Pluvial Event" of Europe. The duration of the disconformity between the Yangliujing and the overlying Zhuganpo formations is unknown, but the reversed polarity of uppermost Yangliujing Formation suggests that the top might correlate with the reversed-polarity zone of the uppermost Ladinian and that the disconformity encompasses the majority of the normal-polarity-dominated *D. canadensis* ammonoid zone.

is equivalent to the reversed-polarity high-GR interval of the basal 20 m of the Xiaowa Formation at Wayao; and (3) the onset of increased silt content in the upper part of the sampled section at Hanwang has expanded the reversed-polarity zone that overlies a pair of normal-polarity zones. This pair of normal-polarity zones is bracketed by two relative peaks in GR at both Wayao and at Hanwang (dashed green lines in Fig. 7a). In order to test this speculative correlation, the magnetostratigraphy at both Wayao and Hanwang needs to be extended upward in the future to search for additional distinctive features, such as a polarity zone of relatively long duration. Our study can only conclude that the magnetostratigraphy and other features of the lower part of the clastic-rich facies in the Hanwang section could be coeval with the lower Xiaowa Formation. The magnetostratigraphy patterns are consistent with the proposal that there was a simultaneous termination of the shallow-water carbonates followed by an influx of clay and other siliciclastics at both the southern and western margins of the Yangtze Platform.

The cyclostratigraphy and '405-kyr envelopes' on '100-kyr GR peaks' in the three Guizhou sections enable depth-to-time conversion of the 210-m-thick Wayao composite magnetostratigraphy into a magnetic polarity time scale spanning ~2.4 my in time (Fig. 7b; correlation guided by dashed green lines). The very brief normal-polarity bands within the Zhuganpo Formation at Wayao interpreted by Montgomery et al. (2003), and in Minzoni et al. (2015) await verification, but the cycle-tuned durations for the main polarity pattern is our target reference scale.

4.2. Testing age-model options for the Carnian

There are two main end-member age models for the Carnian. The choice partly depends on whether the polarity zones of the Julian substage through the lowermost Tuvalian substage, as compiled by Hounslow and Muttoni (2010) from a synthesis of ammonoid- and conodont-dated magnetostratigraphy studies, have equivalents in the cyclostratigraphy-tuned geomagnetic time scale derived from the Newark basin (Fig. 1).

Based upon the published (albeit slightly conflicting) conodont and ammonoid datums, our 2.4-my composite Wayao geomagnetic polarity scale overlaps a significant portion of this critical upper Julian through the lowermost Tuvalian substage interval. A major feature in the composite is the 1.3-my reversed-polarity zone with only very brief normal-polarity excursions in the upper Zhuganpo and the lowermost Xiaowa formations, which is recorded or partly verified in all three Guizhou sections. Its biostratigraphic age is generally assigned as middle or upper Julian. This long reversed-polarity zone is preceded by a 0.3-my zone dominated by normal polarity, underlain by a ~0.55-my one dominated by reversed polarity.

The Julian has a significant reversed-polarity-dominated interval spanning the upper half of the *Trachyceras aonoides* ammonoid zone through lower half of the *Austrotrachyceras austriacum* zone (Figs. 1, 8 and/or A.2). The next younger significant reversed-polarity zone is potentially the *Tropites dilleri* zone, but only if its "unknown" lower part consists of reversed polarity. The current biostratigraphic age assignment to the Zhuganpo Formation as middle or upper Julian would imply that the 1.3-my reversed polarity zone of Wayao corresponds to the *T. aonoides*-*A. austriacum* polarity zone (Fig. 8). This match implies that the rapid transition from limestones of the Zhuganpo Formation to the laminated clay-rich facies of the Xiaowa Formation occurs in the middle of the *A. austriacum* zone. Therefore, it is coeval with the biostratigraphic age of the beginning of the mid-Carnian "Wet Intermezzo" or "Carnian Pluvial Event" of the Germanic Basin and the termination of the shallow-water carbonate platforms of the Dolomites and Austrian Alps.

Is there a potential match of the cycle-scaled Wayao polarity zones of the Julian substage to the cycle-scaled Newark magnetic polarity reference scale? Such a correlation seems difficult to justify. The lowest reversed-polarity zone of relatively long duration in the Newark geomagnetic polarity time scale is Chron E8r, which spans approximately 1.5 my (e.g., Olsen and Kent, 1999) (Fig. 1). This would be the only potential candidate of the Newark succession to correlate with the Wayao 1.3-my reversed-polarity zone and adjacent features. However,

constraints from potential matches of the following reversed-polarity-dominated interval of Chrons E9r–E12r to Carnian–Norian magnetostratigraphy (e.g., options in Fig. 1) seem to require that the age of Chron E8r is either equivalent to the “unknown magnetostratigraphy” of the *Tropites dilleri* ammonoid zone (“Long-Tuvalian option”) or within the lower Norian (“Short-Tuvalian option”). Shifting the age of Chron E8r even further to be late Julian, thereby matching the Wayao 1.3-myrs reversed-polarity interval, would cause problems in finding matches for the distinctive Chron E9r–E12r pattern in the published Tuvalian magnetostratigraphy from marine sediments (e.g., Fig. 1). Alternatively, the assignment of the Zhuganpo Formation to the Julian substages is incorrect, and it should be significantly younger. However, there is no biostratigraphic evidence that it might be Tuvalian or Norian in age.

Therefore, the fit that is most consistent with the Zhuganpo and lower Xiaowa biostratigraphy is the “Short-Tuvalian option” for Carnian and early Norian. This implies that both the composite magnetostratigraphy of Wayao and the entire Julian substages are stratigraphically earlier in the Carnian than the oldest magnetic polarity chron of the Newark Basin magnetic polarity series (Fig. 8).

Based on facies oscillations in the “Carnian Pluvial Event” record in continental and shelfal deposits, this episode has been interpreted as encompassing either two or three 405-kyr cycles, therefore spanning 0.8 or 1.2 myr (e.g., Preto and Hinnov, 2003; Kozur and Bachmann, 2010; Roghi et al., 2010). Based on our cyclo-magnetostratigraphy and correlations to the Julian substages, our Wayao composite does not yet extend high enough to encompass 0.8 to 1.2 myr into the Xiaowa Formation, but it would suggest that the laminated clayey Lower Member (formerly Wayao Formation) of the Xiaowa may span the duration of this mid-Carnian Event.

5. Conclusion

Our combined magnetostratigraphy and cyclostratigraphy study of expanded sections of middle Carnian basinal facies near the margins of the Yangtze Platform has accomplished three main objectives. These objectives were partly achieved by adding cyclostratigraphy and an upward extension to a previous extensive magnetostratigraphy study in the lower portion of one of our Guizhou sections (Montgomery et al., 2003; Minzoni et al., 2015).

- (1) The integrated scale of magnetostratigraphy, spectral-gamma-ray intensity, biostratigraphy and cyclostratigraphy indicates that the lower half of the Zhuganpo Formation of carbonate facies is mixed polarity, followed by a 1.3-myrs dominance of reversed polarity that continues into the clay-rich facies of the lowermost levels of the Lower Member of the Xiaowa Formation, and with mixed-polarity in the remainder of this Lower Member. The onset of clay-rich facies marking the final phase of termination of the Yangtze Platform is approximately synchronous between its southern (Guizhou) and northwest (Sichuan) margins.
- (2) We correlate this distinctive 1.3-myrs reversed-polarity-dominated chron to the long middle Carnian reversed-polarity zone that encompasses the upper half of the *Trachyceras aonoides* through lower half of the *Astrotrachyceras austriacum* ammonoid zones (Hounslow and Muttoni, 2010) (Fig. 8). This conclusion is

consistent with the biostratigraphic constraints from conodonts and ammonoids in these South China formations, and implies that the onset of clay-rich facies occurs in the middle of the *A. austriacum* ammonoid zone in Europe. Therefore, the termination of the Yangtze Platform and initial influx of clastic-rich facies was during the latest Julian and is coeval with the “Wet Intermezzo” or “Carnian Pluvial Event” of the Germanic Basin and with the mid-Carnian influx of clastics that disrupted the shallow-water carbonate platforms in the Italian Dolomites and Austrian Alps regions. This second conclusion can be tested by obtaining cycle-tuned magnetostratigraphies from the European and other “Mid-Carnian Event” reference sections to enable a detailed inter-regional correlation and by acquiring a reliable verified carbon-isotope stratigraphy for the South China facies.

- (3) The distinctive 1.3-myrs reversed-polarity-dominated chron recorded in South China does not have an apparent match to the oldest part of the astronomically-tuned Newark Basin magnetic polarity reference scale. Therefore, the “Short-Tuvalian” age model option with its long-duration Norian stage is the better fit and the oldest part of the Newark Basin polarity scale is within the Tuvalian (late Carnian).

Acknowledgments

We are grateful to the late Heinz Kozur for his detailed education on the mid-Carnian “Wet Intermezzo” and its global implications, and to Marco Franceschi (Univ. Padova, Italy) for a Dolomites stratigraphy field excursion and discussions. Field work was assisted by Zhihao Song, Xueqian Feng and Steve Grasby in Guizhou and by XiongDuan and Yixing Du in Sichuan. Magnetostratigraphy analyses were undertaken at the Black Mountain paleomagnetism laboratory (Australian National University) in Canberra under the patient guidance of David Heslop and Xiang Zhao, and Y.Z.’s stay was funded by the Geologic TimeScale Foundation (USA). Gabi Ogg prepared the time-scale graphics from her diagrams for the GTS2012 volumes and from output from TimeScale Creator (www.tscreator.org). Support for J.O. was from a visiting professorship at the State Key Laboratory of Geobiology and Environmental Geology funded by the Overseas Distinguished Teacher Program of the Ministry of Education (MS2013ZGDZ[WH]028), and as a visiting-scholar sabbatical hosted by the Geosciences Australia (Canberra). Funding for field work, graduate-student support, and international travel costs for Y.Z. and M.L. are from the National Natural Science Foundation of China (nos. 41322013, 41272023, 41272131), the Program for New Century Excellent Talents in University (NCET-11-0723), the Program of Introducing Talents of Discipline to Universities (no. B14031), the China Scholarship Council, and the National Key Basic Research Development Program of China (2012CB822003). ZQC’s work is supported by the 973 Program of China (2011CB808800), the 111 Program of China (B08030), and research grants from the State Key Laboratory of Geobiology and Environmental Geology (GBL11206).

Linda Hinnov and David Heslop generously gave numerous enhancements on informal draft versions. Gerhard Bachmann and an anonymous reviewer provided insightful recommendations on the submitted manuscript and graphics.

Appendix A. Locations and stratigraphy of the Carnian sections

A.1. Geopark Wayao and the Wayao transect (WY); Guizhou province

Geopark Wayao is to the west of the town of Guanling, approximately 150 km SW of Guiyang, the capital city of Guizhou Province (Fig. A.1 WY). In this region, approximately 1000 m of Anisian–Ladinian shallow-water dolomitic limestones of the Guanling and Yangliujing formations are commonly sharply and disconformably overlain by ca. 160 m of biomicritic limestone facies of the Zhuganpo Formation (Figs. A.2, A.3 and

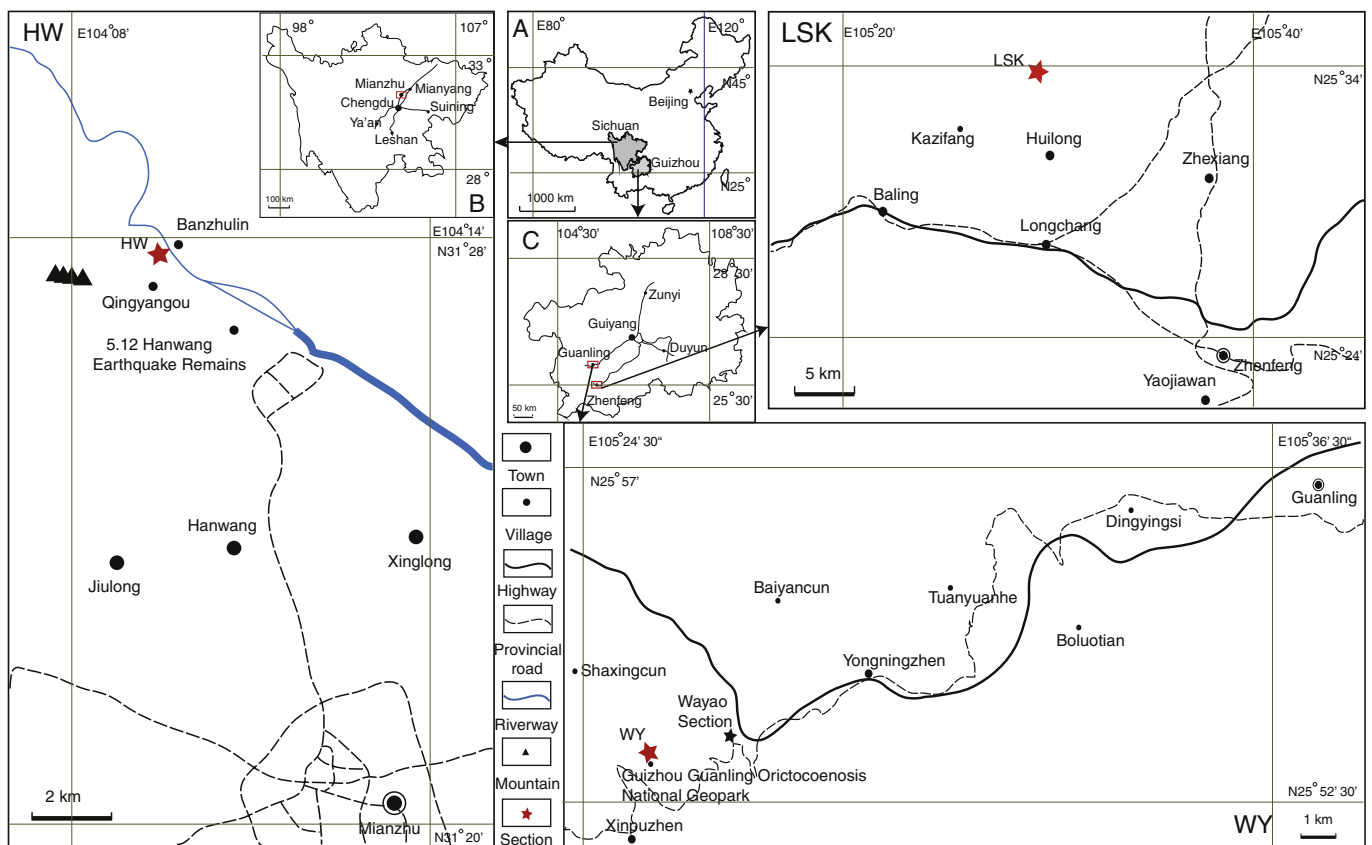


Fig. A.1. Location maps of the magnetostratigraphy and cyclostratigraphy sections. A: Sichuan and Guizhou provinces, China. B and C: Simplified Sichuan Province (section HW) and Guizhou Province (sections WY and LSK) with the sections marked by red stars; HW: Hanwang section ($31^{\circ}27'40''N$, $104^{\circ}9'26''E$, Elevation, 735 m) in Mianzhu, Sichuan; WY: Geopark Wayao section ($25^{\circ}53'34.9''N$, $105^{\circ}25'23.8''E$, Elevation 1337 m) (northeast of the Guizhou Guanling Oricoccoenosis National Geopark), in Guanling, Guizhou, nearby is Wayao section studied by Montgomery et al. (2003), and in Minzoni et al. (2015); LSK: Laishike section ($25^{\circ}33'54''N$, $105^{\circ}29'24.85''E$, Elevation 1177 m), Zhenfeng, Guizhou.

A.4). These disconformity and local hiatus mark the first phase of drowning of the Yangtze Platform on a regional scale (e.g., Minzoni et al., 2015).

The Zhuganpo Formation of medium gray to brown micritic to wackestone limestone contains fossils of thin-shelled pelagic bivalves (e.g. *Halobia*), ammonoids, pseudo-planktonic crinoid *Traumatocrinus*, conodonts, calcispheres, radiolarians, foraminifers and sponge spicules. Rare gastropods and spiriferid brachiopods occur at the base of the formation, and color mottling in the lower part may represent bioturbation. The Zhuganpo Formation is interpreted as a relatively deep-water, dysoxic deposit on the basis of the absence of large, light-dependent biotic biota, fine-grained carbonate texture and lack of winnowing (Minzoni et al., 2015). The influx of micritic carbonate prior to the evolution of pelagic calcareous nannoplankton suggests that there was active shedding of fine-grained carbonate ooze derived from the eastern sector of the surviving portions of the Yangtze Platform (Enos et al., 1998; Minzoni et al., 2015). The age of the Zhuganpo Formation is typically assigned as early Carnian based on the presence of conodont *Metapolygnathus polygnathiformis* throughout the succession with *Metapolygnathus nodosus* of mid-Carnian appearing in the uppermost beds (Wang et al., 2008).

The bedded micritic limestone of the Zhuganpo Formation has a sharp but conformable transition to laminated shale of the mid-Carnian "Wayao Formation" (terminology in Enos et al. (2006)), which has been renamed as Xiaowa Formation by Wang et al. (2008, 2009) (Fig. A.2). The Xiaowa is composed of black, fissile, and slightly calcareous shale. Intercalations of black, thin-bedded, horizontally laminated, pyritic lime mudstone with a hydrocarbon aroma are limited to the lower part of the member. Fossils include ammonoids, thin-shelled pelagic bivalves (*Daonella*, *Halobia*), the pseudoplanktonic crinoid *Traumatocrinus*, driftwood, marine reptiles, fish, conodonts, calcispheres, and foraminifers. Lagerstätte quarries within the laminated Lower Member (ca. 12 m) in the Guanling area contain a wide variety of exceptionally preserved, fully articulated marine reptiles (*Pachypleurosaurus*, *Placodonts*, *Ichthyosauers*, and *Thalattosaurs*; Yin et al., 2000) as well as spectacular clusters of enormous *Traumatocrinus* colonies that have special adaptations to pseudoplanktonic "tow-net" feeding while attached to driftwood (Hagdorn et al., 2007; Wang et al., 2008) that are exhibited in the main Geopark. Interpretations for depositional setting of the Xiaowa Formation, especially the organic-rich Lagerstätte, vary, but Minzoni et al. (2015) conclude that it represents a deep-water anoxic deposit, and that the shut-down in limestone accumulation and shift to exclusively black shale deposition in the upper part of the formation resulted from cessation of input of carbonate ooze as the remaining portions of the Yangtze Platform suddenly drowned.

The Lower Member of the Xiaowa Formation has an overlap of the occurrences of *Protrachyceras* ammonoids that are considered restricted to Early Carnian or younger ages and of the lowest occurrence of *Metapolygnathus nodosus* conodonts that are typically considered to mark the onset of Late Carnian (Wang et al., 2008, 2009), therefore the sharp basal transition is probably the latest Early

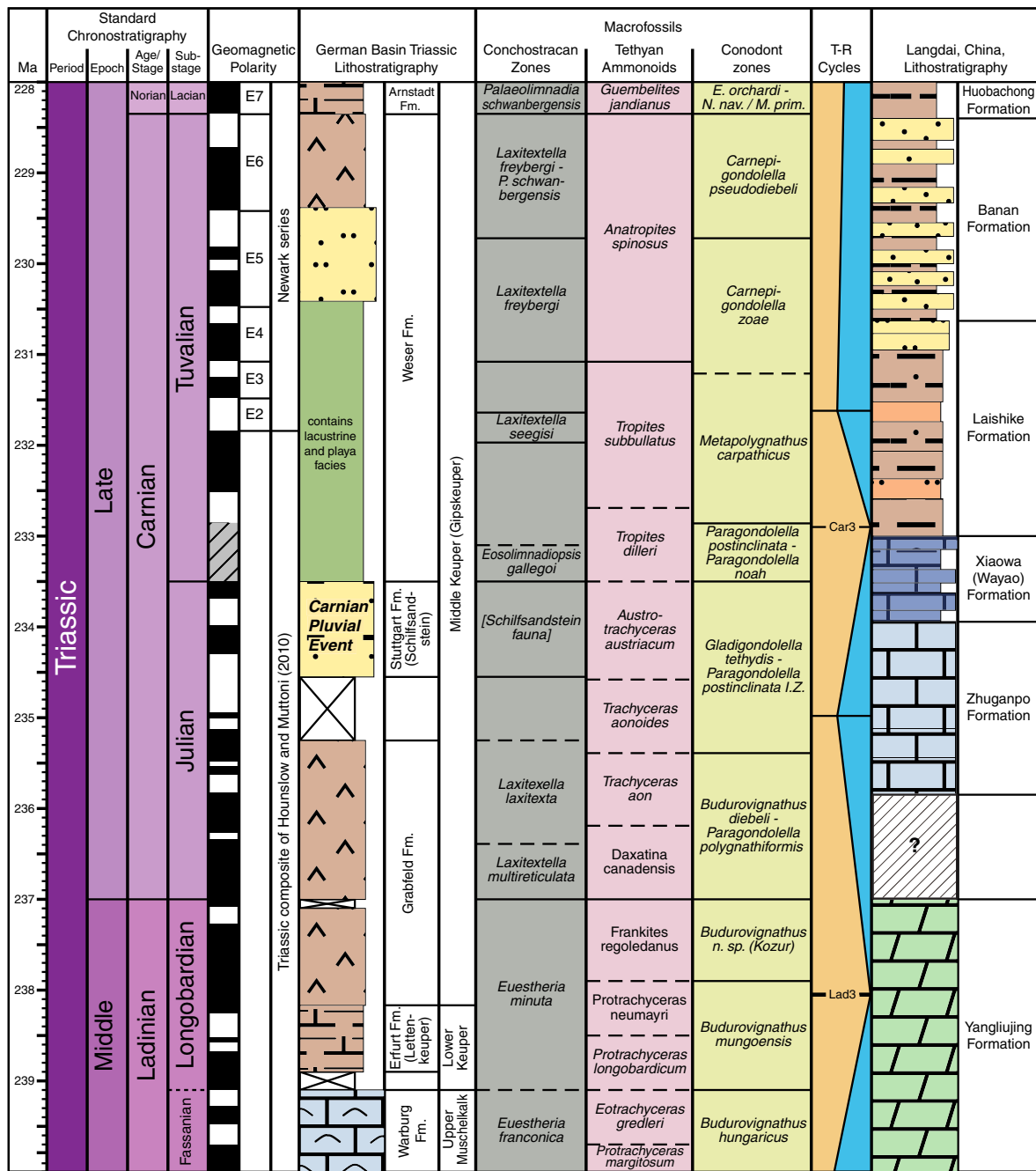


Fig. A.2. Selected Carnian stratigraphic scales. Age model scale and the geomagnetic polarity column are the “Short-Tuvalian” option of Fig. 1. That option had applied an equal-duration ammonoid zone scaling to place events within the Julian substage and had used a possible correlation of the projected ages on the Newark Basin polarity scale (Kent and Olsen, 1999) to the polarity pattern within each Tuvalian ammonoid zone for assigning ages to those ammonoid zones. Geomagnetic polarity pattern within each ammonoid zone of the Julian and Ladinian is modified from the synthesis by Hounslow and Muttoni (2010). The calibrations of this age model and polarity pattern to the other columns are only approximate. Germanic Basin lithostratigraphy with its conchostracean zones are modified from Kozur and Bachmann (2008), Kozur and Weems (2010) and Kozur (pers. comm., 2010). The onset of the Mid-Carnian Event (their “Wet Intermezzo”) in the latest Julian is at the beginning of the sandy Stuttgart Formation. Generalized ammonoid and conodont zones for the Tethyan realm are modified from Kozur (2003, and pers. comm., 2010) and Balini et al. (2010). Major sea-level transgression-regression cycles are modified from Hardenbol et al. (1998) and Haq and Al-Qahtani (2005). Lithostratigraphy of the southern margin of Yangtze Platform is generalized from Enos et al. (2006). The disconformity between the Ladinian dolomitic Yangliujing Formation and the overlying Zhuganpo Formation has an uncertain duration.

Carnian and a candidate for a local response to the Mid-Carnian Event. In contrast, a study of ammonoid assemblages by Xu et al. (2003) had concluded that the lower Xiaowa Formation biota should be assigned to early-Early Carnian according to their interpretation of a *Trachyceras multituberculatum* ammonoid Zone which they correlated to the *T. aon* Zone in Europe; however, the conflict between this suggested ammonoid assignment with the interpreted ages from the conodonts was not resolved in later papers (e.g., Wang et al., 2008, 2009).

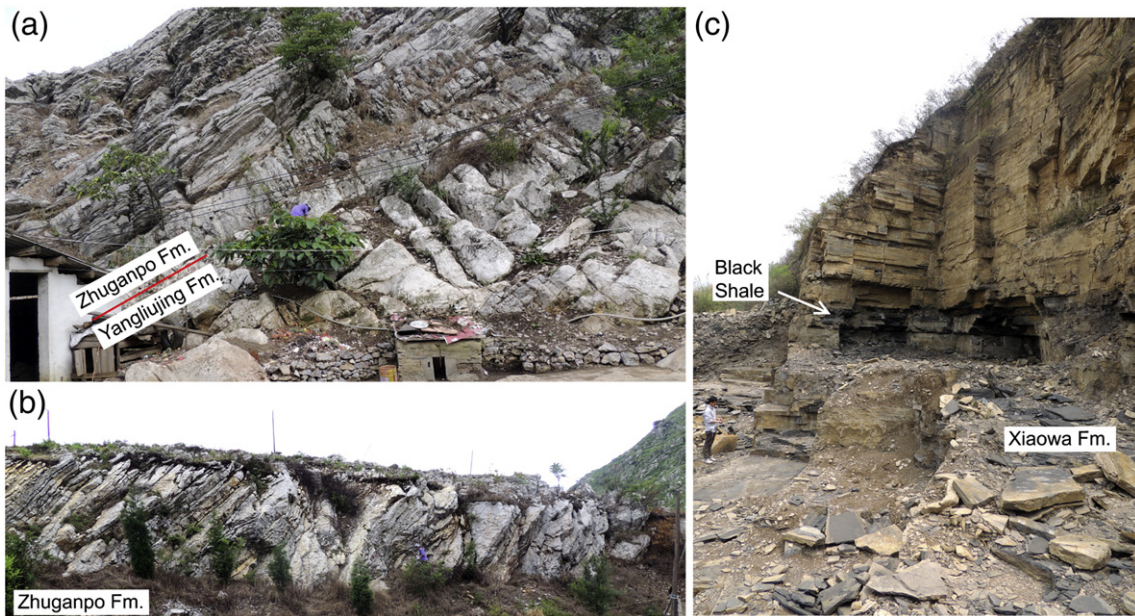


Fig. A.3. Field photos of the WY section. (a) Lower part of the WY section showing the boundary of the dolomitic limestones of the topmost Yangliujing Fm. and thin-bed limestone of the lowermost Zhuganpo Fm. (b) Middle part of the Zhuganpo Fm. with rhythmic beds of limestone. (c) lower Xiaowa Fm. showing black shale interpreted as being within the Middle Carnian Event.

The Xiaowa (Wayao) Formation is conformably overlain by the sandy claystone of the Laishike Formation (Figs. A.3 and A.4). This facies is interpreted as an influx of turbidites with packages of fine-grained sandstone that are fining upward into siltstone and mudstone in partial Bouma sequences (Enos et al., 2006; Lehrmann et al., 2014). The Laishike Formation is 700–800 m thick (Guizhou Bureau, 1987).

Our paleomagnetic sampling during 2014 of the Lower Member and lower half of the Middle Member of the Xiaowa Formation (subdivisions of Wang et al. (2008, 2009)) used fossil quarries on the progressively higher slopes toward the hilltop Geopark museum. Sampling began at the base of a pronounced black-colored interval (Fig. A.3) with a distinct high gamma-ray peak intensity (Fig. A.4) that corresponds to a level at 8.0 m in the middle portion of the Lower Member in the 2005 suite from the Wayao Road exposure; therefore, approximately 15 m of magnetostratigraphy is duplicated between the overlapping studies. There is a gentle anticline through this upward extension, from 12° dip toward 160° in the lower quarry to an average of 4° dip toward due north in the upper hillside quarries.

Detailed gamma-ray intensity measurements were made for cycle stratigraphy in sections (Caishachang, Duimianshan and Wayao Road sections) adjacent to the previous (Montgomery et al., 2003; Minzoni et al., 2015) magnetostratigraphy traverse and through the new (2014) suite. In this process of comparing each feature of the new detailed gamma-ray (GR) transect to the re-located paleomagnetic holes and distinctive features in the previous magnetic susceptibility record, we adjusted for two apparent accidentally skipped intervals in the spliced set of sections in that previous spliced composite section: (1) at the GR – 90 to – 80 level where an apparent discontinuity in their magnetic susceptibility (Minzoni et al.'s 99-m level) seems to be an artifact of projecting to the opposite side of a fold and inadvertently omitting a 10 m interval, and (2) at GR – 45 to – 40 (Minzoni et al.'s 133-m level) where there seems to be an accidental 5-m gap at a shift in their sections. These adjustments bring the distinctive peaks in gamma-ray and magnetic-susceptibility records and placement of paleomagnetic sampling into agreement and are included in the redrawn magnetic polarity graphics in this paper.

This sampling of the dark laminated claystones of 44 m of the lower Xiaowa Formation during 2014 extended upwards by approximately 30 m the previous magnetostratigraphy (Montgomery et al., 2003; Minzoni et al., 2015), which had spanned ca. 150 m of gray to light gray limestone of the complete underlying Zhuganpo Formation and ca. 30 m of the lower Xiaowa Formation. The previous magnetostratigraphy near Wayao indicates that the lower half of the Zhuganpo Formation is mixed polarity, followed by a dominance of reversed polarity that continues into the base of the Xiaowa (Wayao) Formation (Montgomery et al., 2003; Minzoni et al., 2015).

A.2. Laishike (LSK); Guizhou province

The Laishike section in southern Guizhou is approximately 175 km SW from Guiyang city and 50 km south of WY section (Fig. A.1 LSK; Fig. A.5). This mountain-ridge section is within the Nanpanjiang basin, which embayed into the Triassic Yangtze platform. The Ladinian Longtou Formation (marginal facies) is overlain by biomicritic limestone facies of the Zhuganpo Formation of the earliest Carnian (based on conodont assignments by Yang et al. (1995)), followed by a sharp transition to dark-gray clayey laminated carbonates of the mid-Carnian Xiaowa Formation (Fig. A.6) (Wang et al., 2008, 2009). During the late Carnian, there is a gradual transition into a thick succession of silty turbiditic facies of the Laishike and Banan formations. Most of the beds of the relatively porous clay-rich facies of the Xiaowa Formation on this west-facing upper slope of the subtropical agricultural hillside are pervasively weathered to deep levels or not exposed (e.g., distal photograph in Fig. 3 in Wang et al. (2009));

therefore, we concentrated our magnetostratigraphy and cyclostratigraphy studies on the limestones of the Zhuganpo Formation and on the basal part of the Xiaowa Formation exposed within a roadcut. These strata have a uniform dip of ~30° toward the south (184°).

A.3. Hanwang (HW); Sichuan province

In the Longmen Mountains (Longmen Shan) region of Sichuan, China, Middle Triassic platform peritidal carbonates culminate in a lower Carnian facies of oolitic and calcareous sponge facies to nodular-bedded, dark-gray lime mudstone with ammonoids that is suddenly truncated by a mid-Carnian black shale with concentrations of manganese, reduced iron, and organic carbon (basal Ma'antang Formation). The thickness of the black to grayish black shale layer in western Sichuan ranges from 1 to 10 m depending on location (Shi et al., 2009). This “black shale” episode passes into a thick (over 1000 m) terrigenous influx of calcareous siltstone and fine sandstone (Ma'antang Formation) into a flysch to marginal marine setting of late Carnian to Norian. The arrival of this “black shale event” and similar levels in adjacent areas (e.g., Songpan–Garze, Changdu,

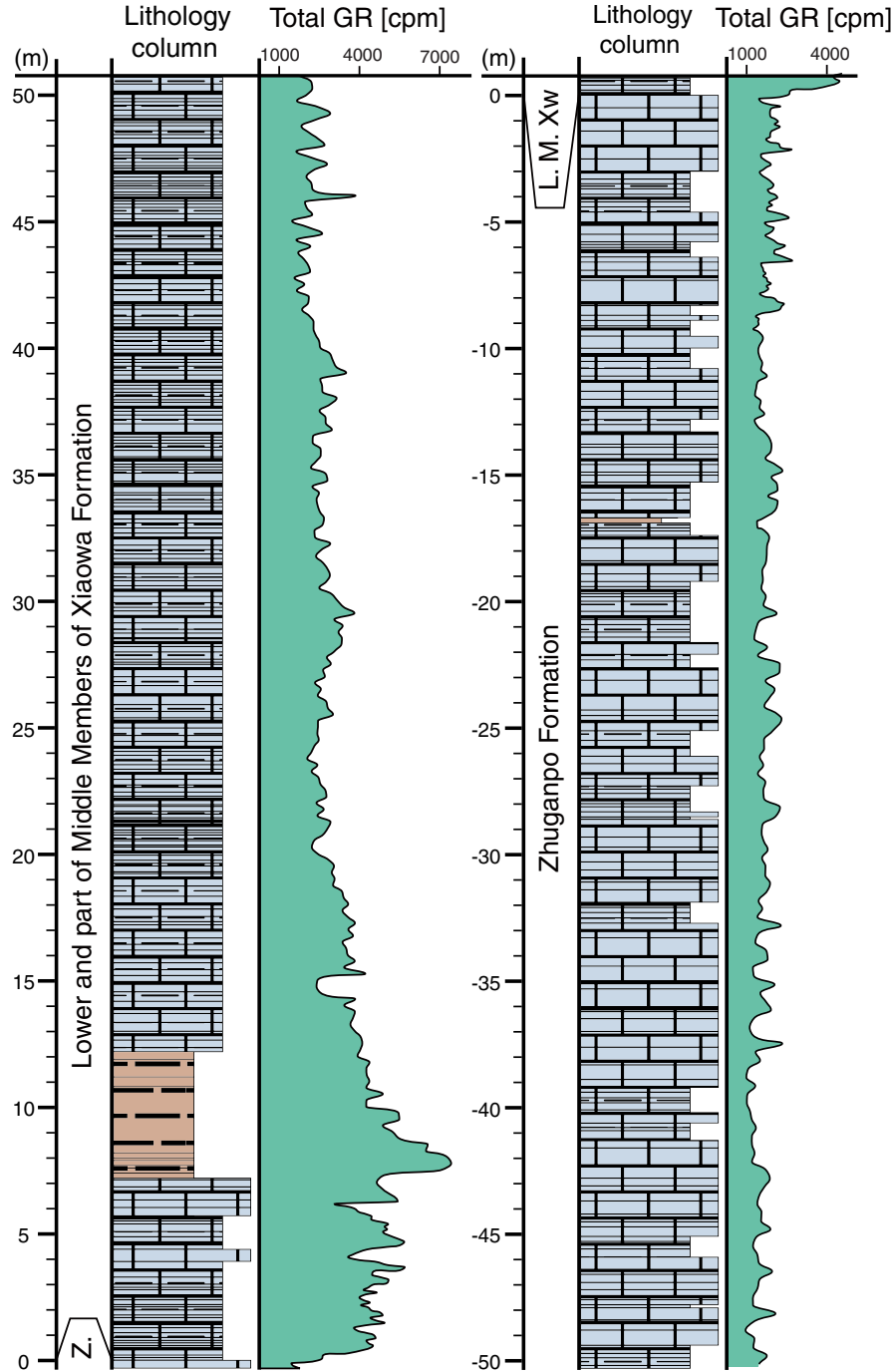


Fig. A.4. Detailed lithology of Wayao section with total gamma-ray intensity log.

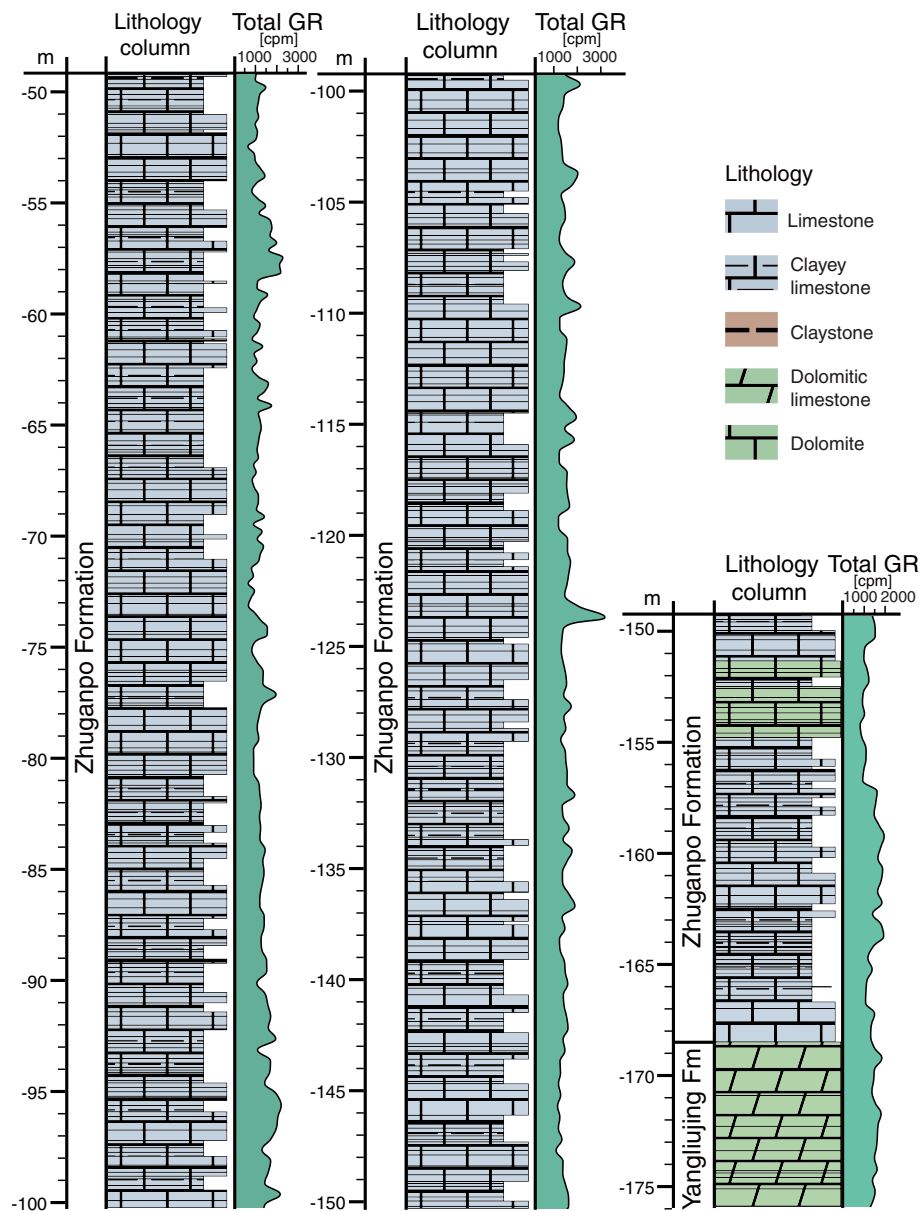


Fig. A.4 (continued).

Hoh Xil) has been proposed as both the cause of the local termination of shallow-water carbonates and the regional response to the mid-Carnian warming (e.g., Shi et al., 2009). However, the termination of this portion of the carbonate platform and influx of clastic sediments has also been interpreted as the development of a Longmen Shan foreland basin during a “Late Longmen Shan” tectonic phase of the general Indosinian collision history as the South China Block and other mini-continents accreted to southern Asia (e.g., Li et al., 2003, 2014; Bradley, 2008). As with all the regional records of the mid-Carnian event, a more precise stratigraphy is required to resolve such multiple interpretations of local versus global factors. Therefore, we sampled 80 m of the Hanwang (HW) section, located just behind the active thrust fault at the base of the Longmen Mountains to the west of the town that was destroyed by the massive Wenchuan 2008 earthquake along this fault line (Fig. A.1 HW; Fig. A.7). The section is approximately 90 km north of Chengdu, the capital city of Sichuan Province. At the HW section, the underlying massive carbonates have a transition into a lower Carnian oolitic limestone and calcareous sponge facies, of which we sampled the uppermost 7 m. This is abruptly overlain by the basal-Ma'antang black-shale layer, followed by a few meters of gray to dark-gray limestone below a very thick unit (>100 m) of silty claystone with some internal cross-bedding and thin (1–3 cm) clay layers (Fig. A.8). The up-thrust strata have an average dip of 45° toward the West (275°).

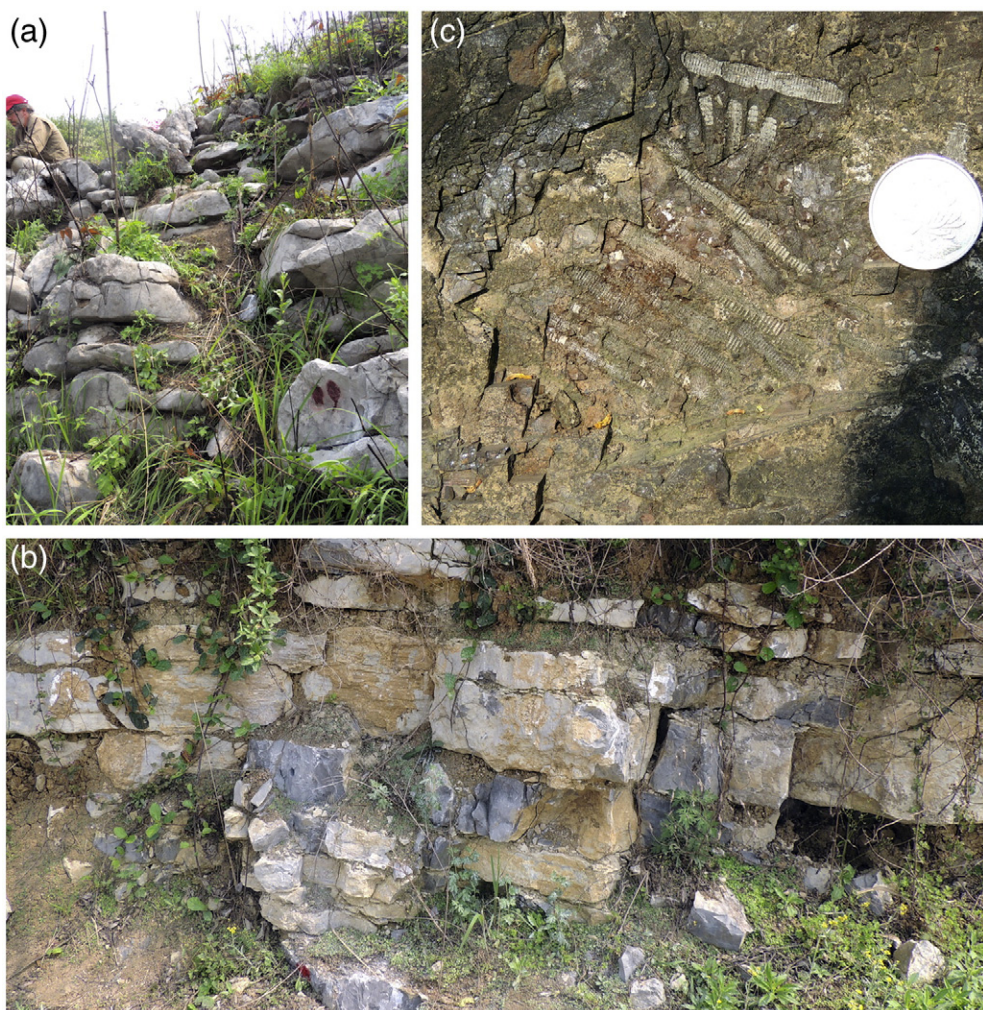


Fig. A.5. Field photos of the LSK section. (a) Limestone of the middle Zhuganpo Fm. of lower part of the section. (b) Rhythmic beds of limestone of the uppermost Zhuganpo Fm. (c) Fragment of a crinoid in the Xiaowa Fm.

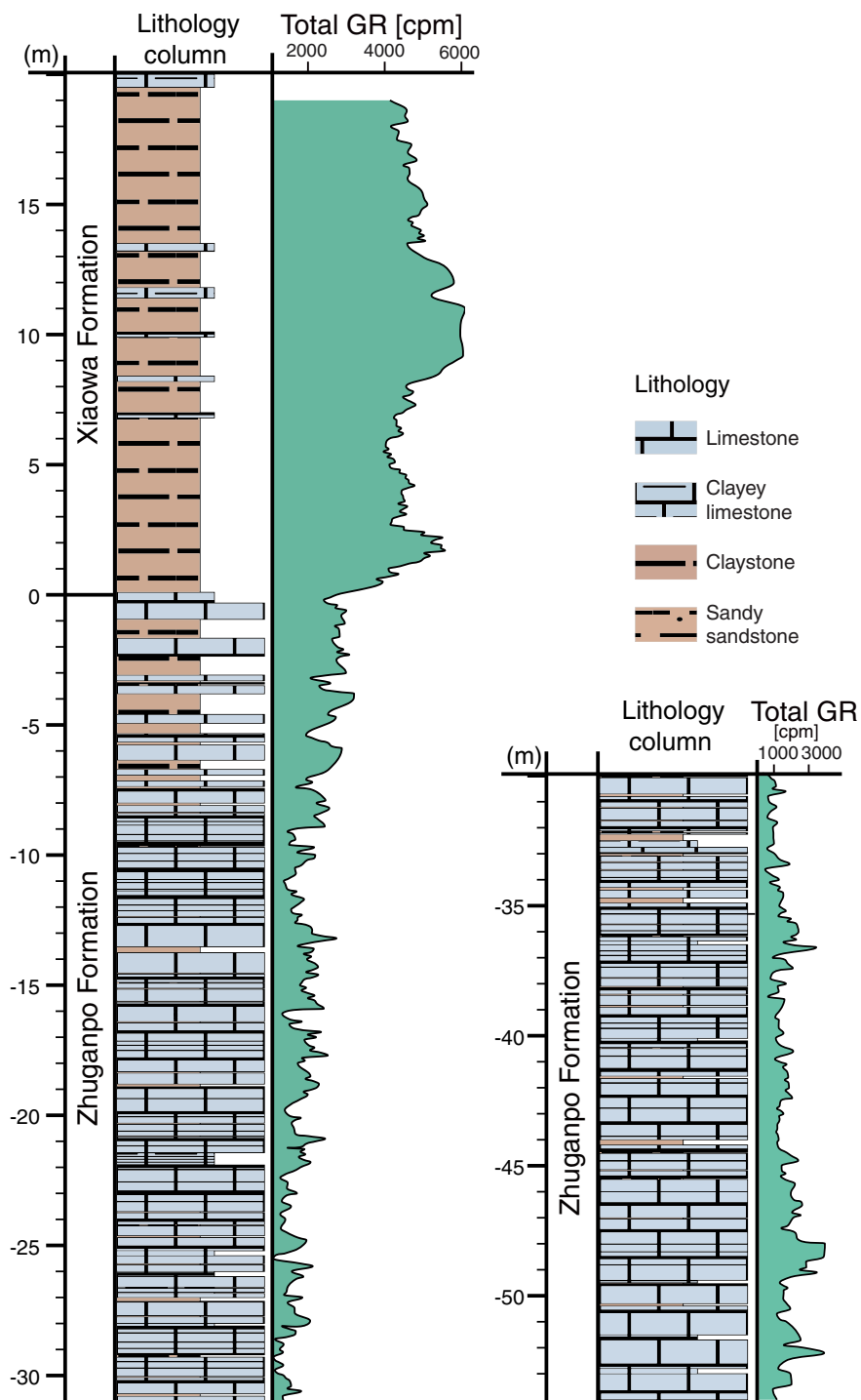


Fig. A.6. Detailed lithology of Laishike section with total gamma-ray intensity log.



Fig. A.7. Field photos of the HW section. (a) Each person is spaced at 10 m intervals. The nearest one (J.O.) points to the first of four shale beds have been interpreted as the local signature of the beginning of the Middle Carnian Pluvial Event (Shi et al., 2009). (b) Closer view of the shale beds with hammer at the lowest shale. (c) Fine to medium sandstones of the Ma'antang Formation in the upper part of the section (67–70 m).

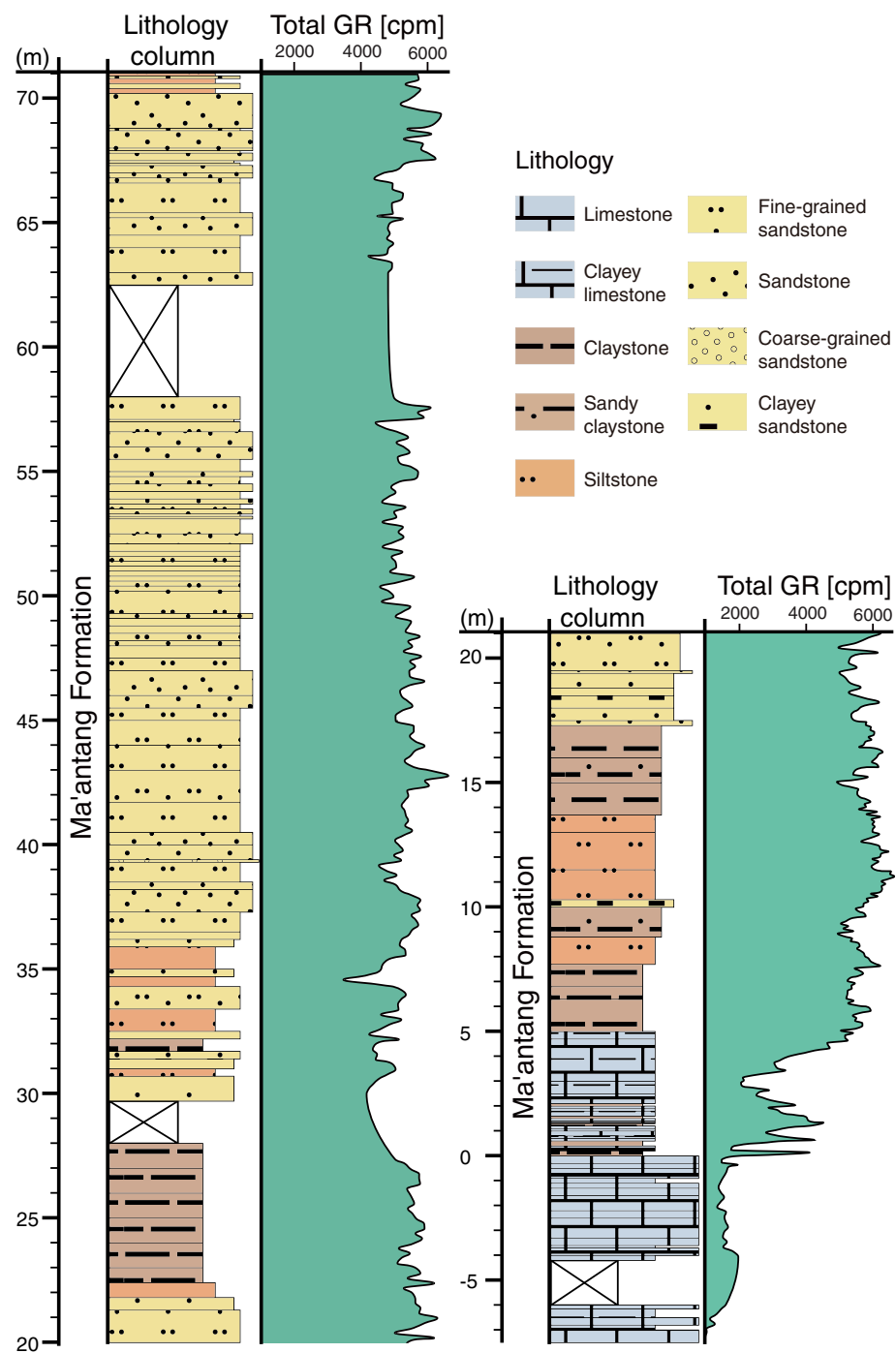


Fig. A.8. Detailed lithology of Hanwang section with total gamma-ray intensity log.

Appendix B. Methodology for cyclostratigraphy and paleomagnetism analysis

B.1. Cyclostratigraphy methods

Stratigraphic variation of total gamma-ray (GR) intensity and its spectral components is a common tool for detecting cyclic facies patterns (e.g., Hesselbo et al., 2009) and for lithologic interpretation and inter-well correlation. A handheld RS-230 BGO Super-SPEC gamma-ray detector was used to measure the GR and the relative contributions from the radioactive isotopes of potassium (K, which is dominated by clay content), thorium (Th, which is especially sensitive to volcanic ash and clay), and uranium (U, which is both influenced by detrital input and organic carbon concentrations). This instrument is reasonably sensitive, but the recorded value at a stratigraphic level is influenced by the gamma-ray emissions from adjacent strata. Therefore, even though the measurement spacing can be fairly narrow (e.g., 10 to 50 cm in our studies), the gamma-ray curves tend to be a smoothed representation of the true variability of K-Th-U throughout a stratigraphic sequence (Ellwood et al., 2013). As a result, when there had been a relatively slow accumulation rate for a sedimentary section, the inherent smoothing of the gamma-ray signals may preclude resolving higher-frequency Milankovitch cycles from precession and obliquity.

The total gamma-ray data were analyzed with the multi-taper method (MTM) for spectral estimation (Thomson, 1982) using both full-section and sliding-window (“evolutive”) intervals. Ratios of the frequency of depth-domain peaks in these spectra were compared to the predicted ratios of time-domain Milankovitch cycles for mid-Triassic (Laskar et al., 2004). The long-term trend was removed from the GR series prior to these spectral analyses. In addition to full spectral analysis, visual examination of the original signal and of band-pass filtering was used to identify distinctive patterns, detect anomalous data points and to highlight potential 405-kyr envelopes on ~100-kyr eccentricity cycles or ~100-kyr envelopes on ca. 20-kyr precession cycles. The position of these gamma-intensity peaks in the depth domain were tagged to a hypothesized cycle frequency (“tuned”) to convert to a time domain using AnalySeries (Paillard et al., 1996). This converted signal was further analyzed using MTM and band-pass filtering to compare to the astronomical parameters.

The untuned gamma-ray signatures also enabled potential correlations among the suite of outcrops. There is an implicit assumption that the sedimentary facies in each section are responding to coeval changes in the influxes of clay, preservation of organic carbon and other components due to regional climatic, oceanographic or sea-level variations. By themselves, these gamma-intensity curves do not always provide a unique fingerprint, but when integrated with magnetic polarity zones, then the combined signal often has a more distinctive signature that can be used for long-distance correlation.

B.2. Paleomagnetic analyses and magnetostratigraphy methods

Paleomagnetic minicores were collected using a gasoline-powered drill and oriented with a magnetic compass in the field. Sample spacing was normally 1 m (90% of samples), but varied from 0.5 m in intervals of major changes in lithology and to up to 3 m spacing in the relatively rapidly accumulating upper Carnian to lowest Norian facies that have only vague biostratigraphy (e.g., upper Laishike Formation). The 2014 sample suite from the three sections consists of 235 drill-plugs (50 at WY, 86 LSK, 99 HW). Montgomery et al. (2003), and in Minzoni et al. (2015) had collected approximately 100 paleomagnetic levels from a total of 190 m in the lower Carnian Zhuganpo and Yangliujing formations below our upward continuation of Section WY.

The lithology of each sample was described after trimming to 2.5-cm cylinders. Carbonate samples were generally light to medium gray, and specimens with more clay were generally dark gray. Approximately 30 samples were not analyzed because these had pervasive weathering to the bases of the minicores.

Each sample (48 WY samples, 70 LSK, 88 HW) was progressively demagnetized in a magnetically shielded room at the Black Mountain Paleomagnetism Laboratory (Australian National University). Remanence measurements were made using a 2G SQUID horizontal pass-through magnetometer equipped with an 8-minicore tray and inline AF demagnetization coils. Each analysis was based on four to six repeat measurements. A conservative percent-error parameter was computed from the statistical deviation with an adjustment for measured residual holder noise after trial runs of a holder that subtracted the baseline holder run. The effective noise level from both sources is equivalent to approximately 1.5×10^{-9} emu/cm³ or 1.5×10^{-3} mA/m [$1 \text{ A/m} = 10^{-3}$ emu/cm³]; implying that a sample with remnant magnetization of 4×10^{-3} mA/m has over 35% noise and hence is our practical limit of no longer statistically useful for polarity interpretations.

An initial alternating-field (AF) step of 5 milli-Teslas (5 mT) was followed by stepwise thermal demagnetization in an ASCTD48SC thermal demagnetizer. Heating involved at least 7 treatments, at ~25 °C steps from 150 °C to 450 °C or 475 °C. Thermal demagnetization was generally ceased because the remnant magnetization displayed either anomalous surges in susceptibility (monitored at each step using a BartingtonMS2 magnetic susceptibility meter), was too weak (less than ca. 5×10^{-3} mA/m) for statistically valid mean directions, or exhibited irregular magnetic directions/intensities for two or three consecutive steps. The choice of a thermal rather than an AF-demagnetization procedure was based upon our preliminary detailed demagnetization pilot run of the main lithologies and the previous work by Montgomery et al. (2003), and in Minzoni et al. (2015) using limestones from section WY.

To further analyze the magnetic minerals that contributed to the magnetic components that were unblocked at different thermal regimes for the gray limestone of the Zhuganpo Formation and the laminated clay-rich facies of the Lower Member of the Xiaowa Formation, Montgomery et al. (2003), and in Minzoni et al. (2015) performed 3-axis Isothermal Remanent Magnetization (IRM) using orthogonal 0.1, 0.3 and 1.2 T fields followed by thermal demagnetization.

A 4-D (space plus intensity) visualization of each sample's magnetic signal through these demagnetization steps, the selection and least-squares calculation of characteristic directions, and the assignment of polarity with a quality annotation was accomplished using the public Paleomagnetic Analysis Program V4.0 (Zhang and Ogg, 2003). Examples of these 4-D views (pair of a modified Zijderveld diagram of both declination-intensity vectors projected onto a horizontal plane with an un-projected curve of inclination-intensity and a Stereographic/Lambert Equal Area projection of the magnetic vector direction) with corresponding interpretations of characteristic directions for typical samples of each polarity and quality-rating are presented in Appendix C (Fig. C.1, Fig. C.2, and Fig. C.3) to this paper. Appendix F contains a full table of all demagnetization results with informal annotations on the polarity interpretations and ratings.

The interpreted polarity and characteristic directions of the samples were given a quality rate of 'N(R)', 'NP(RP)', 'NPP(RPP)', 'N?(R?)' or 'INT' according to a semi-subjective judgment of the behavior of the magnetic vectors through the stepwise demagnetization. Paleogeographic

reconstructions imply that the South China block was at approximately 30°N latitude during the mid-Triassic, and other paleomagnetic studies of Triassic outcrops in the Yangtze Platform and its margins have typically indicated a ~20–35° clockwise post-Triassic rotation for cratonic sites (e.g., Steiner et al., 1989; Enkin et al., 1992; Heller et al., 1995). All samples exhibited a significant overprint of present-day north-pointing magnetic field. Therefore, if the magnetic vectors of a sample trend during progressive demagnetization from this present field direction to stabilize in a direction toward southern declination and upward inclination, and further demagnetization merely decreases the intensity of this vector, then that direction is assigned a high-quality characteristic direction of 'R'. However, as is commonly observed in paleomagnetic studies of clayey limestone facies of Early to Middle Triassic on the South China Block, a more typical behavior is that the magnetization vectors trend away from present-field direction on a great circle or semi-irregular path toward the 'R' or 'N' pole of the cluster of the fewer "well behaved" set of samples (e.g., magnetostratigraphy of lower Triassic at the candidate Olenekian GSSP at Chaochu by Sun et al. (2009), who also used a quality-rating system). In this common case, we applied a 'P' tag of 'RP' or 'NP' when the residual magnetization vector was considered close to attaining an endpoint before losing its residual magnetization or experiencing a surge in susceptibility. The 'P'-rated samples were therefore given only half-weight in computing mean directions for each polarity cluster. The 'PP' tag was applied to samples that had a distinct trend toward the polarity hemisphere to be considered indicative of the underlying polarity, but were judged to be too far from attaining an endpoint before dying to be used in statistics for computing a mean direction. The '?' qualifier was used to denote possible trends toward an underlying polarity, and 'INT' is either entirely uncertain or displayed an endpoint that was intermediate between the 'N' and 'R' poles. All sample magnetic behaviors were interpreted independently by at least two of us (Y.Z. and J.O.); and a conservative compromise was reached during a later discussion.

The mean directions for each polarity with 95% confidence (α_{95}) and clustering parameters of the suites of characteristic vectors were computed with Fisher statistics only on the subsets of samples rated N/NP and R/RP, with those denoted 'P' given half-weight, followed by one iteration that omitted sample directions falling more than 2-sigma (or 60°) from the initial computed mean direction for that polarity. The mean vector intensity for these filtered sample vectors was computed from the log values to partly avoid distortions caused by single high-intensity samples. A site mean vector direction and intensity was computed both by inverting the reversed-polarity sample directions to calculate a combined vector ("Combined" row in Table D.1) and by adding the separate normal- and reversed-polarity vectors ("Vector Comb." row in Table D.1).

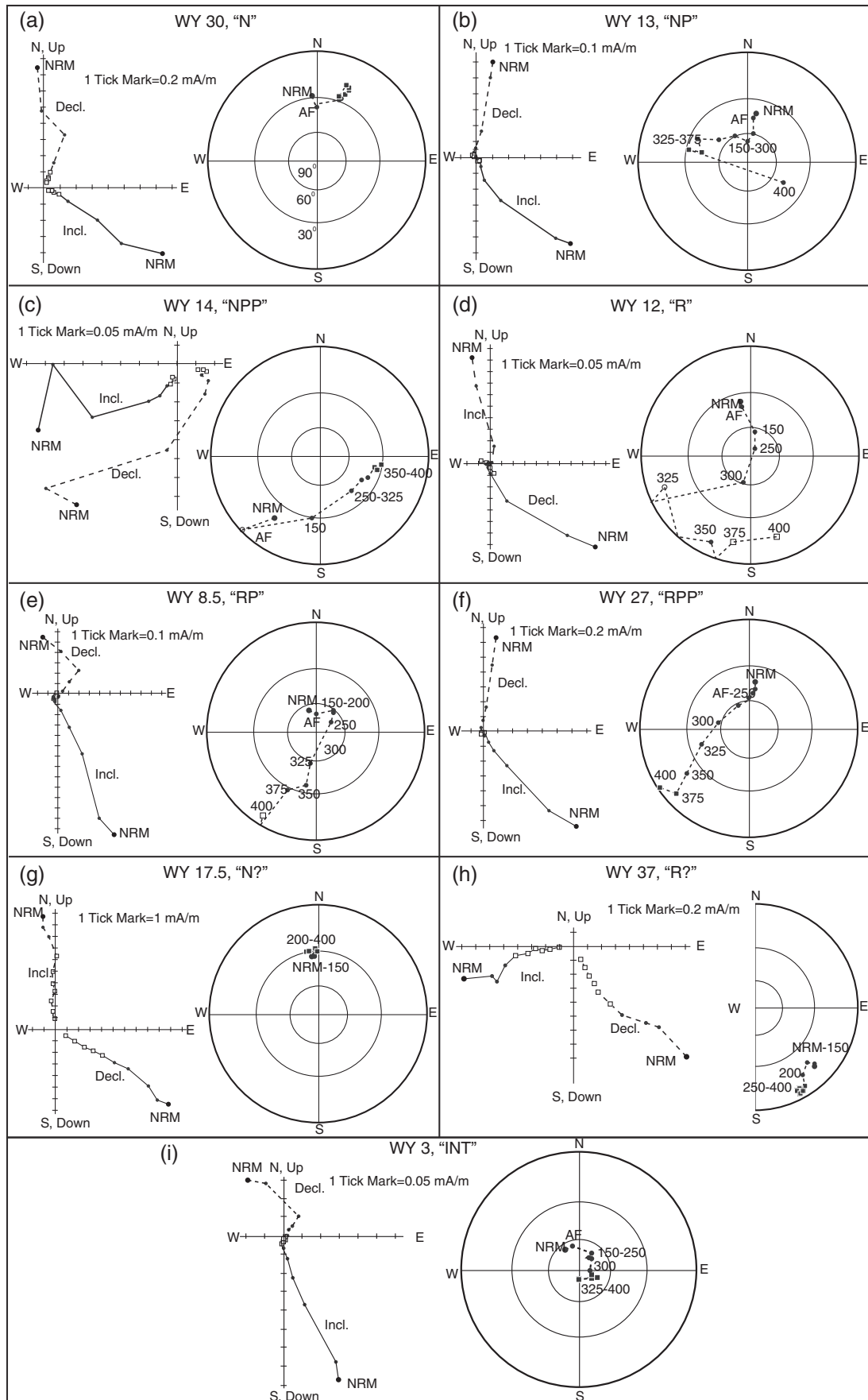
Appendix C. Typical demagnetization behavior for each polarity and quality rating for the Carnian sections


Fig. C.1. Examples of demagnetization plots for different polarities and quality ratings of the Geopark Wayao section (WY), Guizhou during progressive thermal demagnetization after an initial alternating-field step of 5 mT is displayed as stereographic projection (right side of each pair) and projected vector (modified Zijderveld) diagram (left side). Declination (Decl.) and inclination (Incl.) placement in the modified Zijderveld diagrams correspond to the horizontal component and to the projection onto the N-S plane of the vertical component of the magnetization vector (denoted by dashed lines versus solid lines, respectively). In the stereographic projection, the open markers indicate negative inclination. The steps selected for the calculation of the mean characteristic direction are indicated by squares in each plot. (a) Characteristic direction from WY 30 (laminated dark-gray limestone) using the linear decay interval of 300–400 °C is 22.6° Decl., 20.8° Incl. and intensity 0.1 mA/m and is rated “N”. (b) Characteristic direction from WY 13 (gray partly laminated limestone with slightly brownish weathering) using 325–375 °C (before it becomes too weak at 400 °C) is Decl. 289.1°, Incl. 39.4° and intensity of 0.02 mA/m, which is rated “NP” because of the relatively anomalous declination relative to the main normal-polarity cluster (over 60° from the mean normal direction, hence automatically omitted during the second pass of the Fisher statistics computation). (c) Magnetic vectors from WY 14 (laminated gray limestone) display an unusual rotation from an initial downward direction in southern hemisphere to a northeastern endpoint at 350–400 °C. The characteristic direction of this endpoint (100.7° Decl., 32.4° Incl. and intensity 0.08 mA/m) is rated “NPP” because it has the trend the typical cluster of normal-polarity directions but didn’t quite attain that typical northeasterly declination. (d) Magnetic vectors from WY 12 (brownish gray laminated limestone) display a rapid rotation to the reversed-polarity hemisphere, then displayed an increasing intensity at 325 through 400 °C probably due to removing Present-day field overprint. The characteristic direction of 166.2° Decl. and –13.8° Incl. with intensity 0.03 mA/m is therefore rated “R”. (e) Magnetic vectors from WY 8.5 (gray partly laminated limestone) have a progressive trend toward the reversed-polarity hemisphere, but only the last step (400 °C) had attained an associated negative inclination. The selected “characteristic direction” (211.9° Decl., –6.1° Incl. and intensity 0.022 mA/m) was rated as “RP” because it is only that final “best” step. (f) Magnetic vectors from WY 27 (slightly laminated gray limestone) display a similar progressive trend toward the reversed-polarity hemisphere, but the characteristic direction (234.3° Decl., 1.5° Incl. and intensity 0.028 mA/m) from 375 to 400 °C is rated “RPP”. (g) The characteristic direction of WY 17.5 (dark-gray limestone with brownish taint) of Decl. 357.9°, Incl. 29.2° and intensity 3.9 mA/m derived from the 200–400 °C interval is very close to the present field direction and has an anomalously high intensity, therefore it was rated “N?”. (h) The magnetic vectors from WY 37 (laminated gray limestone; but with a weathering stain on top) have a linear segment (250–400 °C) with a characteristic direction of Decl. 149.9°, Incl. 5.9° and mean intensity 0.6 mA/m; however, it was rated “R?” because its stable positive inclination is toward southeast (which is nearly orthogonal to typical clusters of both normal-polarity and reversed-polarity directions) with no indication of a trend. (i) Similarly, the characteristic direction of WY 33 (laminated gray limestone) assigned to the linear decay at 300–400 °C (Decl. 92.2°, Incl. 32.3° and intensity 0.06 mA/m) is rated “INT” from its intermediate direction to either polarity.

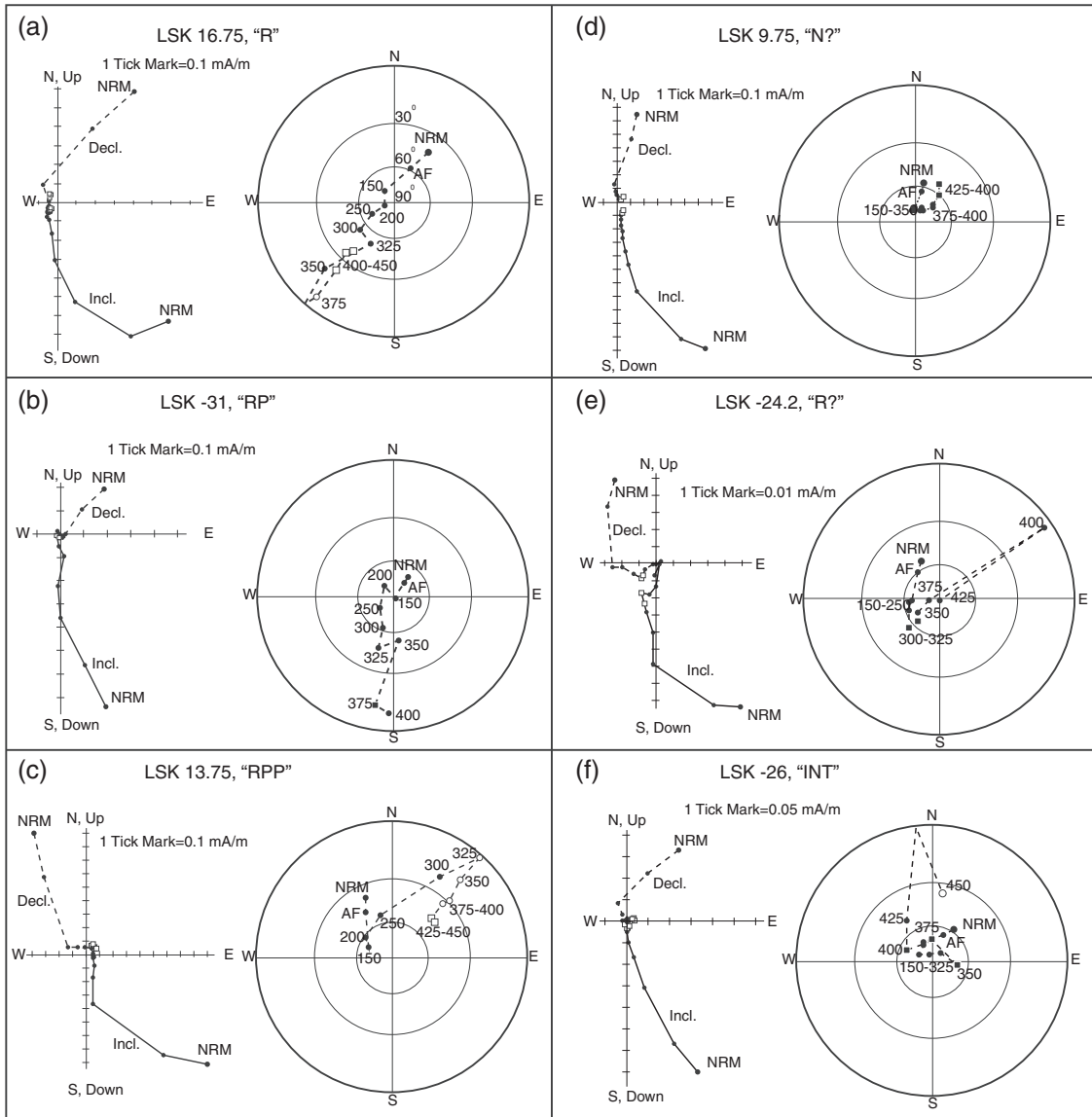


Fig. C.2. Examples of magnetic behaviors for different polarity ratings of the Laishike section (LSK), Guizhou, in same format as Fig. C.1. (a) Characteristic direction from LSK 16.75 (gray limestone with minor brownish weathering) of Decl. 221.7°, Incl. -33.0° is rated “R” due to the progressive trend from present-day field toward the southern hemisphere that reaches a stabilization at 400–450 °C with relatively strong intensity (0.06 mA/m). (b) Magnetic vectors from LSK –31 (gray limestone) display a nice progressive trend from present-day field to a horizontal-South direction and are thus rated “RP” (relative to rest) with 375 °C selected as the best step with Decl. 189.3°, Incl. 10.6° and intensity 0.02 mA/m. (c) Magnetic vectors from LSK 13.75 (gray limestone) trend toward a negative inclination but in a northeasterly declination at 300° through 450 °C. There is no obvious trend toward typical Normal-polarity quadrant, but neither did it reach a typical southern-hemisphere Reversed-polarity direction and is therefore rated “RPP”. The endpoint at 425–450 °C has a mean characteristic direction of Decl. 51.4°, Incl. -44.3° and intensity 0.09 mA/m. (d) Characteristic direction from LSK 9.75 (gray limestone with brownish weathering) of Decl. 39.1°, Incl. 57.7° and intensity 0.09 mA/m is rated “N?” because the magnetic vectors only have an initial trend away from present-day field toward horizontal, but then return to a NRM-type inclination. 425 and 450 °C were selected to represent this sample. (e) The magnetic vectors from LSK –24.2 (gray limestone with slightly reddish weathering) display an initial trend through 300–325 °C away from present-day field to steep-down southwest, but then oddly go to vertical and are therefore rated “R?”. The characteristic direction at 300 and 325 °C is Decl. 226.3°, Incl. 61.7° and intensity 0.02 mA/m; (f) The characteristic direction from LSK –26 (slightly weathered) is Decl. 92.7°, Incl. 73.9° with intensity 0.01 mA/m and rated “INT” because it fluctuated around vertical inclination (350–400 °C selected to characterize this direction), then had a very low intensity at 425 through 450 °C.

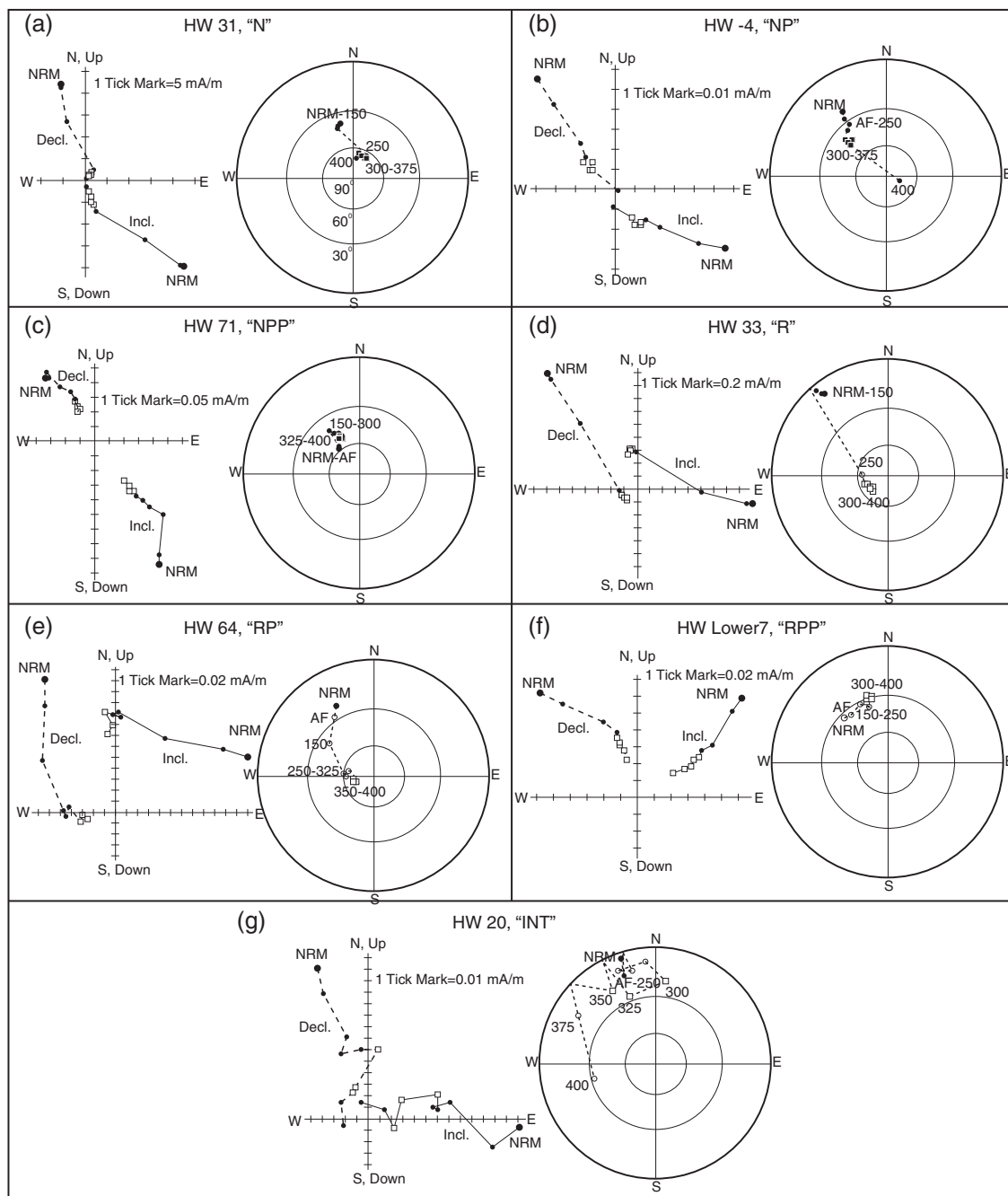


Fig. C.3. Examples of magnetic behaviors for different polarity ratings of the Hanwang (HW) section of Sichuan in same format as Fig. C.1. (a) Characteristic direction from HW 31 (dark-gray limestone with dark speckles) using the linear decay interval of 300–375 °C is Decl. 29.7°, Incl. 67.5° and intensity 4.2 mA/m and is rated “N”. Susceptibility increased at 400 °C. (b) Characteristic direction from HW 4 (gray oolitic limestone) at 300–375 °C is Decl. 311.2°, Incl. 43.9° and intensity 0.02 mA/m. The magnetic vectors shift progressively away from but are still close to present-day field and are thus rated “NP” instead of “N”. (c) The magnetic vectors from HW 71 (gray limestone with silty texture) show no change at 30° rotated northwest from present-day field are rated as “NPP”. The characteristic direction of the endpoint at 325–400 °C is Decl. 331.6°, Incl. 50.1° and intensity 0.02 mA/m. (d) Magnetic vectors from HW 33 (dark-gray limestone with a few shell fragments) a present-day field from NRM to 250° to shift to a stable negative inclination at 300 through 400 °C, and are therefore rated “R” with a characteristic direction Decl. 237.5°, Incl. -69.0° and intensity 0.07 mA/m. (e) Characteristic direction from HW 64 (gray limestone) using 350–400 °C is Decl. 258.1°, Incl. -70.1° with intensity 0.02 mA/m is rated “RP” due to the shift from northwest to stabilize almost due West. (f) The magnetic vectors from HW Lower-Bed7 (brown-tinted gray limestone with light speckles) are rated as “RPP” the 300–400 °C interval yielding a mean characteristic direction of 342.1° (Decl.), -31.5° (Incl.) with intensity 1.9 mA/m. (g) The magnetic vectors from HW 20 (very dark gray limestone) are very noisy and therefore are rated “INT”. Essentially, present-day field is removed until susceptibility surged at 400 °C.

Appendix D. Stereoplots of NRM and high-quality characteristic directions, and mean directions of each outcrop

Table D.1

Mean directions and virtual geomagnetic poles for Geopark Wayao section (WY), Laishike Section (LSK) and Hanwang section (HW) after bedding corrections. Directions are tabulated for each polarity (if applicable), for combined suite after inversion of reversed-polarity characteristic directions, and for the vector average of the normal-polarity vector and inverted reversed-polarity vector. Number is the number of characteristic directions with ratings of N/NP and R/RP (with P-rated given half-weight) used to compute mean directions for each polarity cluster; Dec (Inc) are the mean stratigraphic declination (inclination) with Intensity being the mean-log intensity of the set of characteristic direction vectors; α_{95} is the confidence level at 95% level; κ is Fisher precision (clustering) parameter; Lat (Long) are the latitude (longitude) of the mean virtual geomagnetic pole; $\delta p/\delta m$ are the semi-axes (parallel/perpendicular, respectively) of the 95% confidence level ellipses on this paleomagnetic pole; Paleo-lat is corresponding paleolatitude of the site. For comparison, the mean directions and mean virtual geomagnetic poles of some selected Triassic paleomagnetic studies in South China are also given. Our mean directions from HW (Sichuan) are interpreted to be distorted by a persistent post-Carnian overprint.

Section	Magnetic directions	Mean direction							Mean virtual geomagnetic pole			
		Number	Dec [°]	Inc [°]	Intensity [mA/m]	α_{95} [°]	κ	Lat [°N]	Long [°E]	δ_p/δ_m [°]	Paleo-lat [°]	
WY (Wayao; Guizhou) Wayao transect (Montgomery et al. (2003) ; Minzoni et al. (2015)) <i>M./Lt. Triassic pole for South China Block of Enkin et al. (1992) projected to Wayao</i>	Normal	9.5	32.5	18.4	0.14	17.0	9.6	55.2	217.8	9.2/17.6	9.4	
	Reversed	7	193.7	-14.7	0.05	32.0	4.5	-67.3	68.1	16.7/32.7	-7.3	
	Combined	16.5	24.8	16.9	0.09	15.5	6.5	60.8	227.1	8.2/16.0	8.6	
	Vector average	16.5	27.6	17.4	0.09	-	-	58.8	223.4	8.3/16.0	8.9	
	Combined	216	31.9	37.7		3.3	8.2	60.4	198.0	2.3/3.9	21.13	
M./Lt. Triassic pole for South China Block of Enkin et al. (1992) projected to Wayao	5 sites	48	34		16.8			45.1	194.4	$\alpha 95 = 16.8$	18.6	
	Reversed	11.5	213.5	-29.7	0.05	23.8	4.5	-57.3	26.0	14.6/26.4	-15.9	
LSK (Laishike; Guizhou) HW (Hanwang; Sichuan)	[Equiv. N]	11.5	33.5	29.7	0.04	23.8	4.5	57.3	206.0	14.6/26.4	15.9	
	Normal	22	350.7	62.8	0.46	4.9	41.0	75.3	76.8	6.0/7.7	44.2	
	Reversed	28	253.3	-60.5	0.26	7.5	14.2	-31.9	342.0	8.7/11.4	-41.4	
	Combined	50	38.7	67.7	0.33	6.6	10.2	55.7	148.9	9.3/11.1	50.6	
	Vector average	50	20.1	67.8	0.34	-	-	65.7	136.1	9.3/11.1	50.7	
<i>Comparison with selected Triassic paleomagnetic studies in Sichuan region</i>												
NE Sichuan (Shangsi) Lt. Perm-E. Triassic (Heller et al. (1988))	Combined		35.9	12.8		2.2		47.9	225.1	1.14/2.24	6.5	
NE Sichuan (Shangsi) Lt. Perm-E. Triassic (Steiner et al. (1989))	Combined	38	36.4	12.2		4.5	32.7	47.2	226.3	2.1/4.2	6.2	
E. Sichuan Lt. Perm-E. Triassic (Heller et al. (1995))	3 sites	42.7	15.0					44.3	217.4	$\alpha 95 = 3.5$	7.6	
E. Sichuan (Hechuan) E. Triassic (Steiner et al. (1989))	Uni-vectorial subset	62	50.4	17.1		3.5	33.5	38.5	209.8	1.7/3.3	8.7	

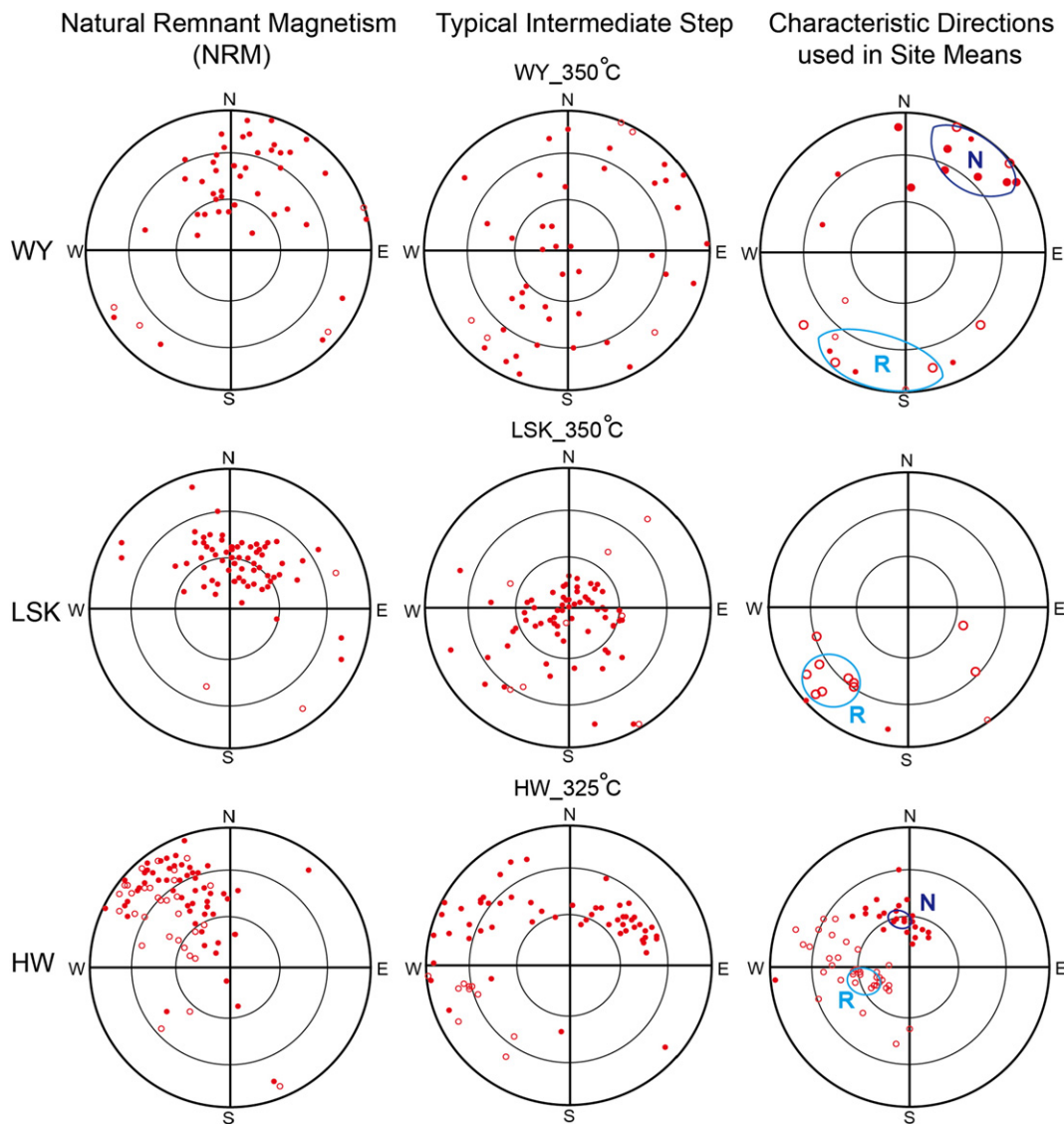


Fig. D.1. Tilt-Corrected stereoplots of the initial natural remnant magnetism (NRM) and the 350 °C demagnetization step, which is a typical intermediate step on great-circle paths as magnetic vectors rotate toward opposing endpoint directions, characteristic directions for all samples with N-NP- and R-RP-rating used in computation of mean directions for Geopark Wayao Section (WY, with average dip of 12° toward 160°), Laishike Section (LSK, with average dip of 30° toward 184°) and Hanwang Section (HW, with average dip of 45° toward 275°). The ovals are the approximate 95% confidence circles on the mean directions of characteristic directions for each polarity (see Table D.1).

Appendix E. Details of cyclostratigraphy and magnetostratigraphy interpretations of each section

The details of the cyclostratigraphy and magnetostratigraphy of the composite section from Wayao are given in the main text. This Appendix gives the explanations of the cyclostratigraphy and magnetostratigraphy for the Laishike (LSK) and Hanwang (HW) sections, plus additional diagrams and statistics for the Wayao (WY) sections.

E.1. ASM results of Wayao cyclostratigraphy

The ASM method (Meyers and Sageman, 2007) provides a test for rejecting the null hypothesis (no orbital signal) and objective estimation of the optimal sedimentation rate for a stratigraphic interval that was influenced by astronomical forcing. Considering our mean sampling interval of the Yangliujing and Zhuganpo formations at Wayao (0.35 m/measurement), we examined the frequency from 0 to 1.5 cycles/m above 99% confidence level for ASM estimate. Null hypothesis significance level shows that the optimal accumulation rate is ~10.0 cm/kyr (ASM = 0.0027 cycles/kyr; H_0 significance level = 0.31%) (Fig. E.1). Besides, the accumulation rate is the only value that exceeds the critical significance lever of 0.567%. In addition, the null hypothesis (H_0 , no orbital forcing) could be rejected with a high degree of confidence (probability < 0.31%).

E.2. Laishike (LSK) section – magnetostratigraphy and cyclostratigraphy

The magnetic behaviors of many of the samples from the limestones of the Zhuganpo Formation and the laminated clay-rich to homogeneous sandy carbonates of the Xiaowa Formation at the Laishike are generally similar to these lithologies at Wayao. The remnant magnetization upon demagnetization at 450° or above was generally at levels near the noise-level of the ANU magnetometer. Polarity was partly interpreted from the progressive drift of magnetic vectors during thermal demagnetization to this limiting temperature. In general, the drift was approximate along segments of great circles away from the common initial NRM clustering at ~55° toward the north, which we interpret as an initial strong overprint of present magnetic field. The bedding dip of 30° toward the south implied that this overprint in stratigraphic coordinates is steeply downward (ca. 85°) toward the north, therefore quite distinct from the shallow inclinations (ca. 25–50°) predicted for the normal-polarity directions of Carnian strata. Characteristic directions of the majority of the LSQ samples were largely computed from the vectors at the 350° to 425 °C thermal steps. Due to the persistence of a significant present-day field component onto the primary magnetization, we relaxed the criteria for quality ratings – “R” assigned if the great-circle trend has a characteristic direction or endpoint in the southern hemisphere with negative inclination; “RP” if nearly horizontal inclination in the southern hemisphere; and “N” or “NP” if there is both a great-circle trend with a final characteristic direction an inclination less than ca. 60° in the northern hemisphere. The directions of the few samples that attained these relaxed quality ratings were all of reversed polarity and, surprisingly, when inverted to normal-polarity direction these yielded a mean (34° declination, 30° inclination, but with alpha-95 of 24°; Table 1) that is consistent with the mean normal-polarity direction (33° declination, 18° inclination; alpha-95 of 17°) of section WY. However, a significant fraction (ca. 40%) of the characteristic directions was judged as questionable or indeterminate (INT) polarity due to a persistence of this present-day field overprint (Fig. D.1 LSK, and gray-shading in Fig. E.2). A few samples had a great-circle path segment that suggested possible drift toward the expected normal-polarity pole; however, because none attained an inclination less than 55° compared to the ca. 20–35° inclination that is expected for Carnian-age sediments, these were given a low quality rating (“N?”). Therefore, the magnetostratigraphy of the Laishike section based on the higher-quality samples is entirely of reversed polarity (Fig. E.2).

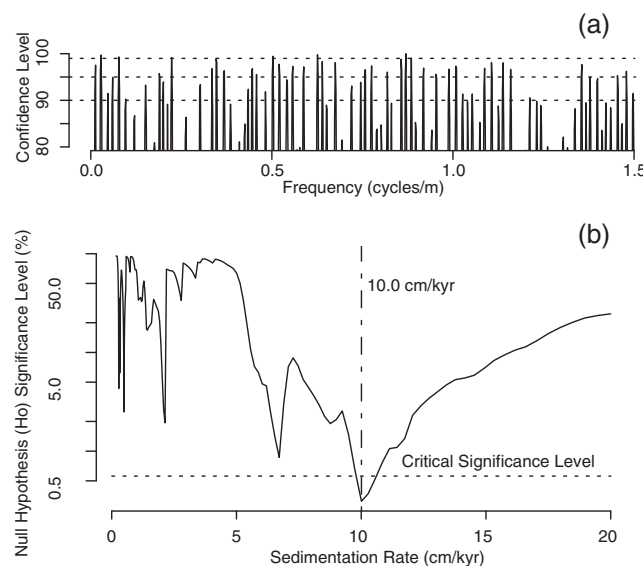


Fig. E.1. ASM results of SGR series of the lower-middle Wayao section. (a) MTM harmonic spectral analysis and confidence level of the GR series of the mid-lower part of the Wayao section (from –176 m to 0 m, Yangliujing and Zhuganpo formations). The SGR series are after removing a 80-m-averaged trend using a Matlab script ‘floess’ (robust locally weighted linear least squares and 2nd degree polynomial model). (b) Null hypothesis significance level for accumulation rates from 1 to 20 cm/kyr with a 0.1 cm/kyr increment of the Wayao section from –176–0 m. The dashed line indicates the critical significance level.

The GR curve for the Zhuganpo Formation displays two low broad peaks centered at about -15 and -50 m below the base of the high-gamma Xiaowa Formation. Sliding-window spectral analysis of the 80-m-thick section indicates an important ~ 10 -m oscillation under this possible ~ 34 -m cycle, and with another statistically-significant cycle at 1.9 m.

Despite the 50-km distance between WY and LSK outcrops, the two sections display the same dominance of reversed polarity, the identical cyclicity (ca. 34, 10 and 1.9 m; Fig. E.3) and correlation of the main GR trends for the upper 55 m of the Zhuganpo and the basal 25 m of the Xiaowa formations.

E.3. Hanwang (HW) section in Sichuan – magnetostratigraphy

The initial NRM vectors of the clayey and silty facies of HW cluster toward the present field direction. Progressive thermal demagnetization from 150° through 300°C causes a distinct migration of the magnetic vectors into two distinct clusters. After correcting for the 45° stratigraphic dip toward the west, one cluster has negative inclinations with western declinations and a second with positive inclinations toward the northeastern declinations (Fig. D.1 HW). Even though these two clusters are not antipodal, neither are near the initial present-field overprint, therefore these were interpreted as reversed-polarity and normal-polarity orientations, respectively. Most samples display stable characteristic directions with declining intensity from 325° through 400°C , then either become too weak to reliably measure or begin to display erratic jumps in magnetization vectors with a surge in susceptibility. The means of the R/RP-rated samples (253° declination, -61° inclination) and of the N/NP-rated samples (351° declination, 63° inclination) are not antipodal and are comparably steeper than the Carnian directions from the Guizhou sites (Fig. D.1 HW; Table D.1). The mean "N" vector has nearly twice the intensity of the "R" vector. This suggests that there was a persistent residual overprint component on most samples, and that demagnetization at higher temperature steps caused a simultaneous decrease of that overprint component that was generally in-step with the decline in the remnant intensity of the primary Carnian vector. Therefore, even though the separation into stratigraphic intervals of alternating polarity is quite evident for approximately two-thirds of the samples, the mean directions for both polarities are steepened by this persistent overprint and are not a reliable indicator of the Carnian field. A relaxed quality rating of 'R' was reserved for the characteristic directions of sample magnetization vectors that had stable end-points in the southern hemisphere, and 'RP' assigned for those that distinctly moved toward the 'reversed cluster' but appeared to have a degree of residual overprint that precluded a full drift into the southern hemisphere before the onset of susceptibility surges (Fig. C.3).

The stratigraphic clustering of the interpreted characteristic directions and polarity ratings in the clastic-rich portion of the Ma'antang Formation indicates a dominance of reversed polarity with 3 well-delineated normal-polarity bands (Fig. E.4). The total gamma intensity (GR) curve has a broad peak at the 10 m to 20 m stratigraphic interval corresponding to a reversed-polarity zone. The overlying clastic-rich facies has subtle features in the GR that correspond to general finer-grained lithologies (e.g., the GR spikes at ca. 22–27 m, 45 m and 70 m levels). The oolitic limestones underlying the Ma'antang Formation are normal polarity with a low GR.

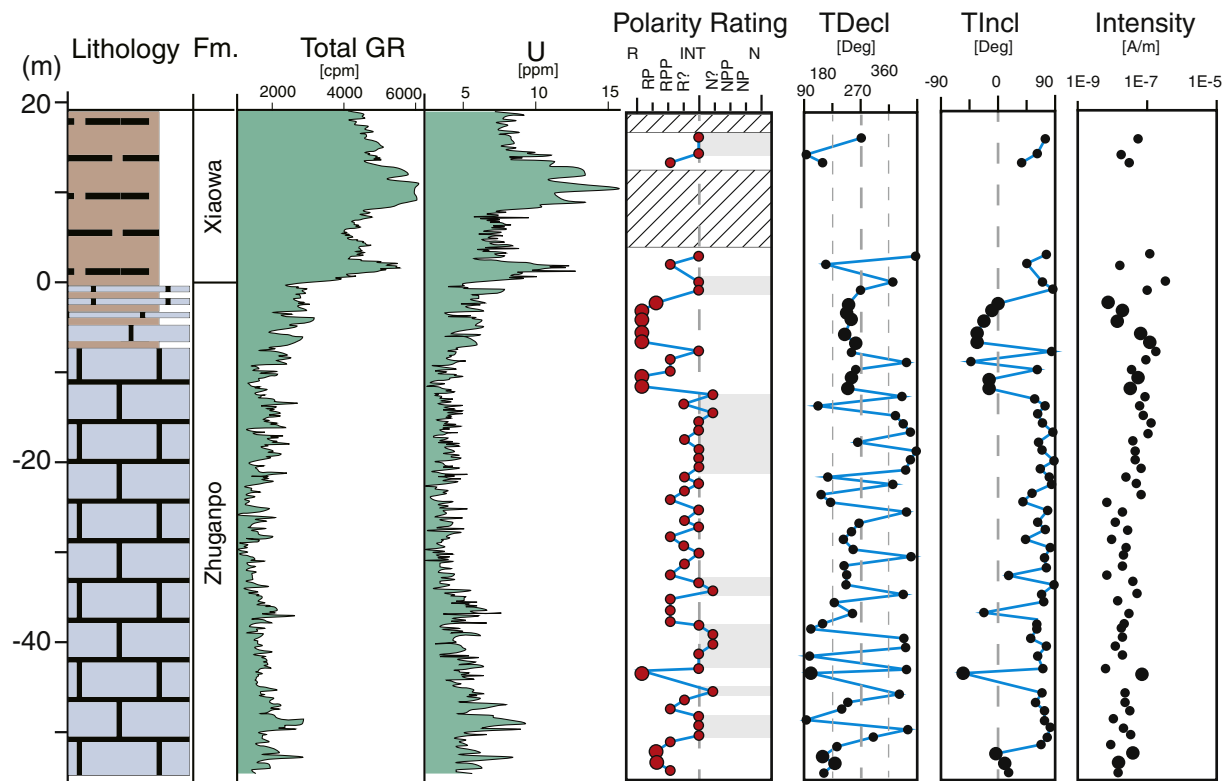


Fig. E.2. Magnetostratigraphy of the Laishike section with total (GR) and U-spectra gamma-ray intensity. The peaks of the GR and U correspond to laminated, very dark gray, clay-rich levels. In the polarity column, the gray shading indicates intervals where polarity ratings were all "?" or "INT"; but there are no definite normal-polarity intervals in this section. Polarity rating (N to INT to R) as explained in Appendix B has superimposed black bars for normal polarity, white bars for reversed polarity and gray bars for sample gaps or clusters of indeterminate and intermediate (INT) vectors. Declination-inclination-intensity values are for the vectors computed by least-squares from the characteristic magnetization steps in stratigraphic (bedding tilt-corrected) coordinates. Larger dots indicate the N/NP- and R/RP-rated vectors used in the computation of mean directions.

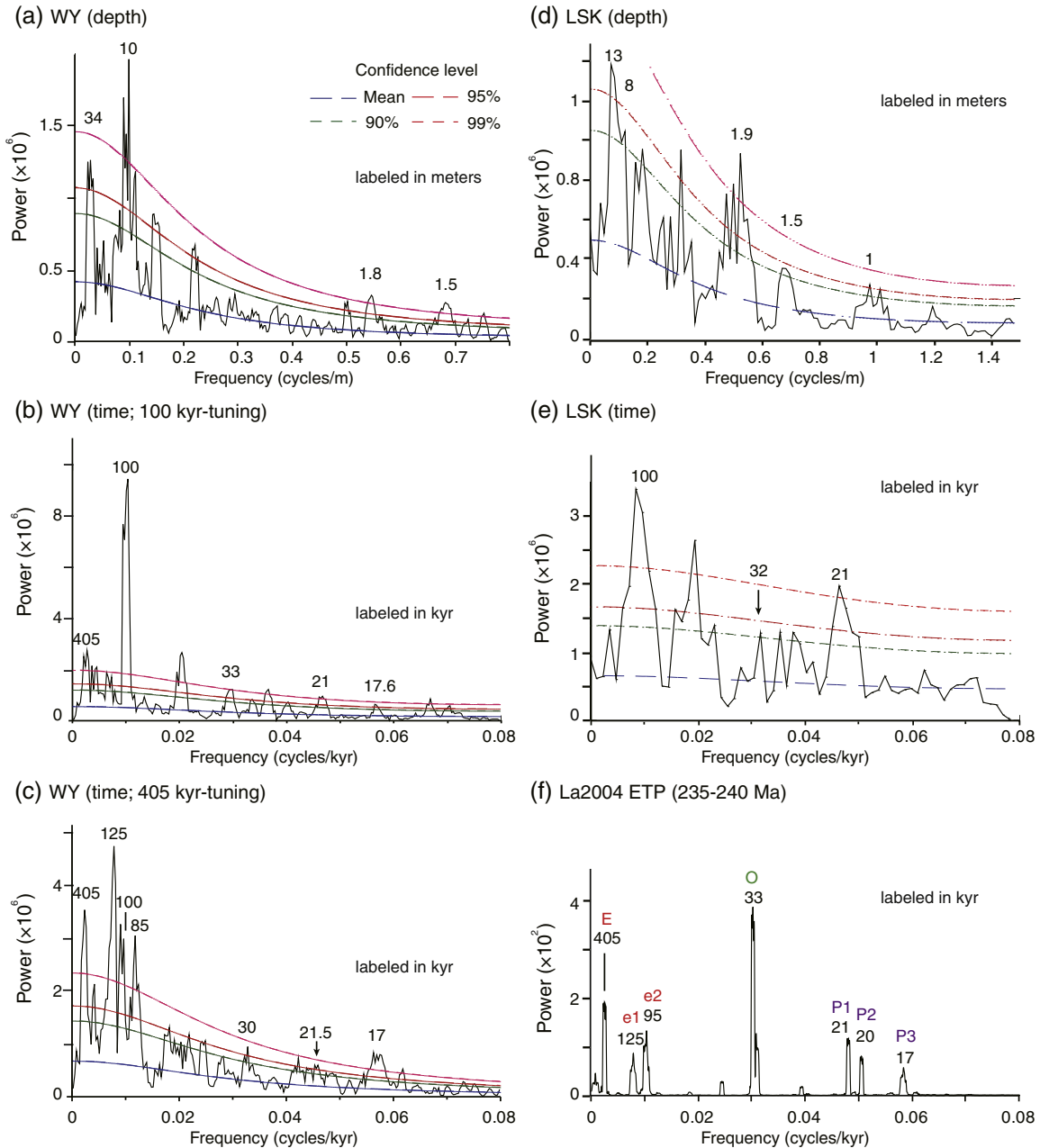


Fig. E.3. Spectral analysis. (a) 2π MTM power spectrum of the total WY GR series from -176 m to 50.6 m, after removing the 80-m lowess trend. (b) 2π MTM power spectrum of the 100 kyr tuned total WY GR used in (a). (c) 2π MTM power spectrum of the 405 kyr tuned total WY GR used in (a). (d) 2π MTM power spectrum of the total LSK GR series from -54.5 m to 2 m, after removing the 35-m lowess trend. (e) 2π MTM power spectrum of the 100-kyr tuned GR series used in (c). (f) The La2004 model from 235 to 240 Ma (Laskar et al., 2004) showing predicted astronomical-cycle frequencies (E = long eccentricity, e = short eccentricity, O = obliquity, P = precession) for early Carnian age. A robust red noise model is calculated with linear fitting and a median smoothing window bandwidth about 20% of the effective Nyquist frequency range of each series.

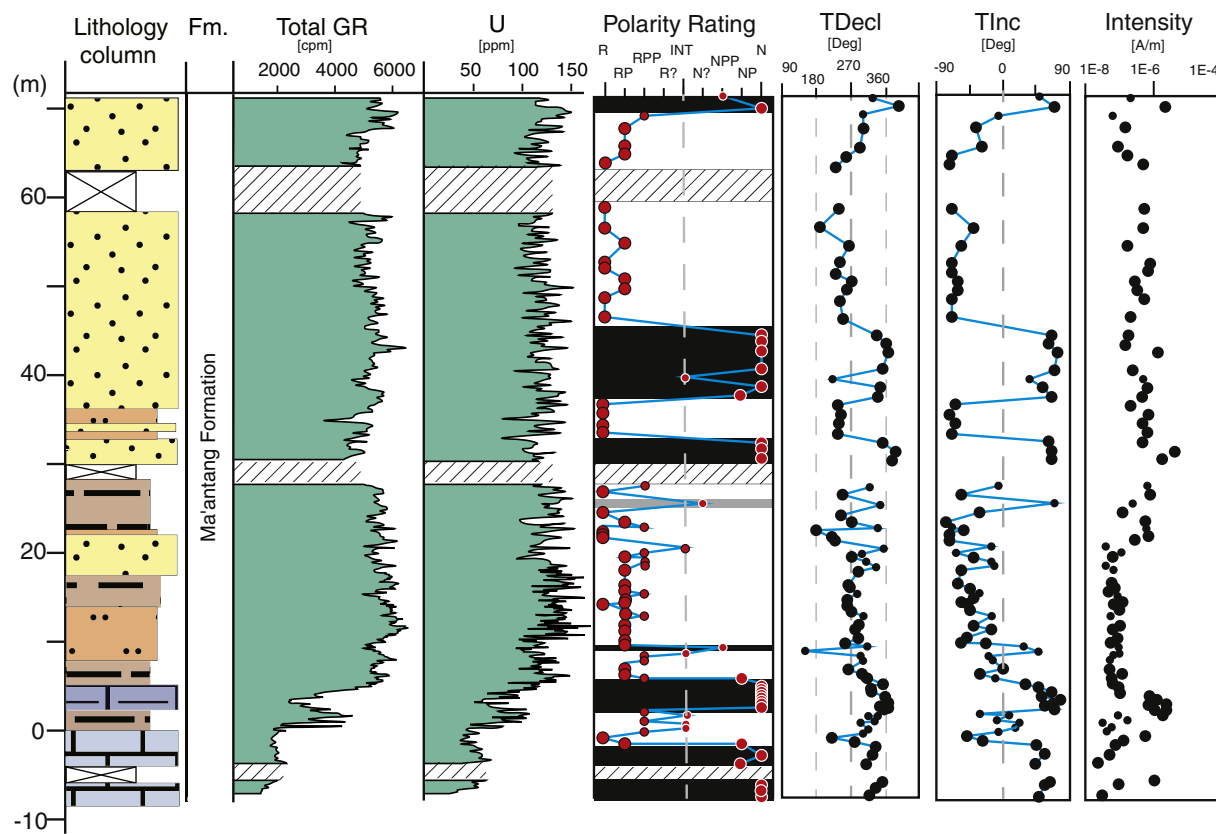


Fig. E.4. Magnetostratigraphy of the Hanwang section with total (GR) and U-spectra gamma-ray intensity. The peaks of the GR and U correspond to laminated, very dark gray, clay-rich levels. See Fig. E.2 for explanation of column formats.

Appendix F. Supplementary data

Appendix F. Excel table of all paleomagnetic demagnetization data with comments on paleomagnetic analysis and the raw GR data (see the separate file "Appendix F. mid-Carnian workbook.xlsx"). Supplementary data to this article can be found online at <http://dx.doi.org/10.1016/j.palaeo.2015.05.033>.

References

- Balini, M., Lucas, S.G., Jenks, J.F., Spielmann, J.A., 2010. Triassic ammonoid biostratigraphy: an overview. *Geol. Soc. Lond. Spec. Publ.* 334 (1), 221–262.
- Besse, J., Torcq, F., Gallet, Y., Ricou, L.E., Krystyn, L., Saidi, A., 1998. Late Permian to Late Triassic palaeomagnetic data from Iran: constraints on the migration of the Iranian block through the Tethyan Ocean and initial destruction of Pangaea. *Geophys. J. Int.* 135 (1), 77–92.
- Bradley, D.C., 2008. Passive margins through earth history. *Earth Sci. Rev.* 91 (1–4), 1–26.
- Dal Corso, J., Mietto, P., Newton, R.J., Pancost, R.D., Preto, N., Roghi, G., Wignall, P.B., 2012. Discovery of a major negative ^{13}C spike in the Carnian (Late Triassic) linked to the eruption of Wrangelia flood basalts. *Geology* 40 (1), 79–82.
- Dong, W., Lin, S., Chen, Y., Yin, G., Jiao, H., Wang, K., Wang, H., Gan, X., Zhang, J., Xu, H., 1997. Stratigraphy (lithostratigraphic) of Guizhou Province. China University of Geosciences Press, Wuhan, pp. 1–306.
- Ellwood, B.B., Wang, W.-H., Tomkin, J.H., Ratcliffe, K.T., El Hassani, A., Wright, A.M., 2013. Testing high resolution magnetic susceptibility and gamma radiation methods in the Cenomanian-Turonian (Upper Cretaceous) GSSP and near-by coeval section. *Palaeogeogr. Palaeoclimatol. Palaeoecol.* 378, 75–90.
- Enkin, R.J., Yang, Z., Chen, Y., Courtillot, V., 1992. Paleomagnetic constraints on the geodynamic history of the major blocks of China from the Permian to the present. *J. Geophys. Res. Solid Earth* 97 (B10), 13953–13989.
- Enos, Paul, Jiayong, Wei, Lehrmann, D.J., 1998. Death in Guizhou – Late Triassic drowning of the Yangtze carbonate platform. *Sediment. Geol.* 118, 55–76.
- Enos, P., Lehrmann, D.J., Jiayong, W., Youyi, Y., Jiafei, X., Chaikin, D.H., Minzoni, M., Berry, A.K., Montgomery, P., 2006. Triassic evolution of the Yangtze Platform in Guizhou Province, People's Republic of China. *Geol. Soc. Am. Spec. Pap.* 417, 1–105.
- Feng, Z., Bao, Z., Li, S., 1997. Lithofacies Paleogeography of the Middle and Lower Triassic of South China. Petroleum Industry Press, Beijing, pp. 1–222.
- Golonka, J., 2007. Late Triassic and Early Jurassic palaeogeography of the world. *Palaeogeogr. Palaeoclimatol. Palaeoecol.* 244 (1–4), 297–307.
- Greene, A.R., Scotes, J.S., Weis, D., Katvala, E.C., Israel, S., Nixon, G.T., 2010. The architecture of oceanic plateaus revealed by the volcanic stratigraphy of the accreted Wrangellia oceanic plateau. *Geosphere* 6 (1), 47–73.
- Gu, X., Liu, X., 1997. Stratigraphy (lithostratigraphic) of Sichuan Province. China University of Geosciences Press, Wuhan, pp. 1–417.
- Guizhou Bureau of Geology and Mineral Resources, 1987. Regional Geology of Guizhou Province: Geological Memoires, Ser. 1, no. 6, 700 p. (Geologic map 1:500,000).
- Haggdorn, H., Wang, X., Wang, C., 2007. Paleoecology of the pseudoplanktonic Triassic crinoids *Traumatocrinus* from southwest China. *Palaeogeogr. Palaeoclimatol. Palaeoecol.* 247 (3–4), 181–196.
- Haq, B.U., Al-Qahtani, A.M., 2005. Phanerozoic cycles of sea-level change on the Arabian Platform. *GeoArabia* 10 (2), 127–160.
- Hardenbol, J., Thierry, J., Farley, M.B., Jacquin, Th, de Graciansky, P.-C., Vail, P.R., 1998. (with numerous contributors), Mesozoic and Cenozoic sequence chronostratigraphic framework of European basins. In: de Graciansky, P.-C., Hardenbol, J., Jacquin, Th, Vail, P.R. (Eds.), Mesozoic-Cenozoic Sequence Stratigraphy of European Basins. SEPM Spec. Publ. 60, pp. 3–13 763–781.
- Heller, F., Lowrie, W., Huamei, L., Junda, W., 1988. Magnetostratigraphy of the Permo-Triassic boundary section at Shangsi (Guangyuan, Sichuan Province, China). *Earth Planet. Sci. Lett.* 88 (3–4), 348–356.
- Heller, F., Haibong, C., Dobson, J., Haag, M., 1995. Permian-Triassic magnetostratigraphy – new results from South China. *Phys. Earth Planet. Inter.* 89 (3–4), 281–295.
- Hesselbo, S.P., Deconinck, J.-F., Huggett, J.M., Morgans-Bell, H.S., 2009. Late Jurassic palaeoclimatic change from clay mineralogy and gamma-ray spectrometry of the Kimmeridge Clay, Dorset, UK. *J. Geol. Soc.* 166, 1123–1133.
- Hornung, T., Brandner, R., 2005. Biochronostratigraphy of the Reingraben Turnover (Hallstatt Facies Belt): local black shale events controlled by regional tectonics, climatic change and plate tectonics. *Facies* 51 (1–4), 460–479.
- Hornung, T., Brandner, R., Krystyn, L., Joachimski, M.M., Lorenz, K., 2007a. Multistratigraphic Constraints on the NW Tethyan “Carnian Crisis”.
- Hornung, T., Krystyn, L., Brandner, R., 2007b. A Tethys-wide mid-Carnian (Upper Triassic) carbonate productivity crisis: evidence for the Alpine Reingraben Event from Spiti (Indian Himalaya)? *J. Asian Earth Sci.* 30 (2), 285–302.
- Hounslow, M.W., Muttoni, G., 2010. The geomagnetic polarity timescale for the Triassic: linkage to stage boundary definitions. *Geol. Soc. Lond. Spec. Publ.* 334 (1), 61–102.

- Huang, C., Hesselbo, S.P., Hinnov, L., 2010. Astrochronology of the late Jurassic Kimmeridge Clay (Dorset, England) and implications for Earth system processes. *Earth Planet. Sci. Lett.* 289, 242–255.
- Kent, D.V., Olsen, P.E., 1999. Astronomically tuned geomagnetic polarity timescale for the Late Triassic. *J. Geophys. Res. Solid Earth* 104 (B6), 12831–12841.
- Kozur, H.W., 1975. Probleme der Triasgliederung und Parallelisierung der germanischen und tethyalen Trias. Teil II: Anschluß der germanischen Trias an die internationale Triasgliederung. *Freibg. Forsch. C* 304, 51–77.
- Kozur, H.W., 2003. Integrated ammonoid, conodont and radiolarian zonation of the Triassic and some remarks to stage/substage subdivision and the numeric age of the Triassic stages. *Albertiana* 28, 57–83.
- Kozur, H.W., Bachmann, G.H., 2008. Updated correlation of the Germanic Triassic with the Tethyan scale and assigned numeric ages. *Ber. Geol. Bundesanst.* 76, 53–58.
- Kozur, H.W., Bachmann, G.H., 2010. The Middle Carnian Wet Intermezzo of the Stuttgart Formation (Schilfsandstein), Germanic Basin. *Palaeogeogr. Palaeoclimatol. Palaeoecol.* 290 (1–4), 107–119.
- Kozur, H.W., Weems, R.E., 2010. The biostratigraphic importance of conchostracans in the continental Triassic of the northern hemisphere. *Geol. Soc. Lond. Spec. Publ.* 334 (1), 315–417.
- Krystyn, L., 1974. Probleme der biostratigraphischen Gliederung der Alpin-Mediterranen Obertrias. *Schriftenr. Erdwiss. Kommiss. Österr. Akad. Wiss.* 2, 137–144.
- Laskar, J., Robutel, P., Joutel, F., Gastineau, M., Correia, A.C.M., Levrard, B., 2004. A long-term numerical solution for the insolation quantities of the Earth. *Astron. Astrophys.* 428 (1), 261–285.
- Lehrmann, D.J., Chaikin, D.H., Enos, P., Minzoni, M., Payne, J.L., Yu, M., Goers, A., Wood, T., Richter, P., Kelley, B.M., Li, X., Qin, Y., Liu, L., Lu, G., 2014. Patterns of basin fill in Triassic turbidites of the Nanpanjiang basin: implications for regional tectonics and impacts on carbonate-platform evolution. *Basin Res.* 1–26. <http://dx.doi.org/10.1111/bre.12090>.
- Lehrmann, D.J., Enos, P., Payne, J.L., Montgomery, P., Wei, J., Yu, Y., Xiao, J., Orchard, M.J., 2005. Permian and Triassic depositional history of the Yangtze platform and Great Bank of Guizhou in the Nanpanjiang basin of Guizhou and Guangxi, south China. *Albertiana* 33 (1), 147–166.
- Li, Y., Allen, P.A., Densmore, A.L., Qiang, X., 2003. Evolution of the Longmen Shan Foreland Basin (Western Sichuan, China) during the Late Triassic Indosinian Orogeny. *Basin Res.* 15 (1), 117–138.
- Li, Y., Yan, Z., Liu, S., Li, H., Cao, J., Su, D., Dong, S., Sun, W., Yang, R., Yan, L., 2014. Migration of the carbonate ramp and sponge buildup driven by the orogenic wedge advance in the early stage (Carnian) of the Longmen Shan foreland basin, China. *Tectonophysics* 619–620 (0), 179–193.
- Lucas, S.G. (Ed.), 2010. The Triassic timescale. *Geol. Soc. Lond. Spec. Publ.* 334.
- Lucas, S.G., Tanner, L.H., Kozur, H.W., Weems, R.E., Heckert, A.B., 2012. The Late Triassic timescale: age and correlation of the Carnian–Norian boundary. *Earth Sci. Rev.* 114 (1–2), 1–18.
- Meyers, S.R., Sageman, B.B., 2007. Quantification of deep-time orbital forcing by average spectral misfit. *Am. J. Sci.* 307 (5), 773–792.
- Minzoni, M., Lehrmann, D.J., Dezoeten, E., Enos, P., Montgomery, P., Berry, A., Qin, Y., Meiyi, Y., Ellwood, B.B., Payne, J.L., 2015. Drowning of the Triassic Yangtze Platform, South China, by Tectonic subsidence into toxic deep waters of an anoxic basin. *J. Sediment. Res.* 85 (5), 419–444 (Magnetostratigraphy included in online Appendix available at <http://sepm.org/pages.aspx?pageid=229>).
- Montgomery, P., Enos, P., Lehrmann, D.J., Wei, J., Ellwood, B.B., 2003. Post mortem in Guizhou: Rates and reasons of post-drowning deposition. AAPG Annual Meeting, May 11–14, 2003, Salt Lake City, Utah (abstract available at http://www.searchanddiscovery.com/abstracts/pdf/2003/annual/short_ndx_78240.PDF).
- Nakada, R., Ogawa, K., Suzuki, N., Takahashi, S., Takahashi, Y., 2014. Late Triassic compositional changes of aeolian dusts in the pelagic Panthalassa: response to the continental climatic change. *Palaeogeogr. Palaeoclimatol. Palaeoecol.* 393, 61–75.
- Ogg, J.G., 2012. Chapter 25 – Triassic. In: Gradstein, F.M., Schmitz, M.D., Ogg, G.M. (Eds.), *The Geologic Time Scale*. Elsevier, Boston, pp. 681–730.
- Ogg, J.G., 2015. The mysterious Mid-Carnian “Wet Intermezzo” global event. *J. Earth Sci.* 26 (2), 181–191.
- Ogg, J.G., Huang, C., Hinnov, L., 2014. Triassic timescale status: a brief overview. *Albertiana* 41, 3–30.
- Olsen, P.E., Kent, D.V., 1999. Long-period Milankovitch cycles from the Late Triassic and Early Jurassic of eastern North America and their implications for the calibration of the Early Mesozoic time-scale and the long-term behaviour of the planets. *Philos. Trans. R. Soc. A Math. Phys. Eng. Sci.* 357 (1757), 1761–1786.
- Paillard, D., Labeyrie, L., Yiou, P., 1996. Macintosh Program performs time-series analysis. *EOS Trans. Am. Geophys. Union* 77 (39), 379.
- Preto, N., Hinnov, L.A., 2003. Unraveling the origin of carbonate platform cyclothem in the Upper Triassic Dürrenstein Formation (Dolomites, Italy). *J. Sediment. Res.* 73 (5), 774–789.
- Preto, N., Kustatscher, E., Wignall, P.B., 2010. Triassic climates – state of the art and perspectives. *Palaeogeogr. Palaeoclimatol. Palaeoecol.* 290 (1–4), 1–10.
- Roghi, G., Gianolla, P., Minarelli, L., Pilati, C., Preto, N., 2010. Palynological correlation of Carnian humid pulses throughout western Tethys. *Palaeogeogr. Palaeoclimatol. Palaeoecol.* 290 (1–4), 89–106.
- Scotese, C.R., 2001. *Atlas of Earth history, Volume I. Paleogeography*. University of Texas, Paleomap Project, Arlington (52 pp.).
- Shi, Z., Ou, L., Luo, F., Li, Y., Qian, L., 2009. Black shale event during the Late Triassic Carnian Age: implications of sedimentary and palaeontological records in Longmen Mountains region. *J. Palaeogeogr.* 11, 375–383.
- Simms, M.J., Ruffell, A.H., 1989. Synchronicity of climatic change and extinctions in the Late Triassic. *Geology* 17 (3), 265.
- Simms, M.J., Ruffell, A.H., 1990. Climatic and biotic change in the late Triassic. *J. Geol. Soc.* 147 (2), 321–327.
- Steiner, M., Ogg, J., Zhang, Z., Sun, S., 1989. The Late Permian/Early Triassic magnetic polarity time scale and plate motions of south China. *J. Geophys. Res. Solid Earth* 94 (B6), 7343–7363.
- Sun, Z., Hounslow, M.W., Pei, J., Zhao, L., Tong, J., Ogg, J.G., 2009. Magnetostratigraphy of the Lower Triassic beds from Chaochu (China) and its implications for the Induan-Olenekian stage boundary. *Earth Planet. Sci. Lett.* 279 (3–4), 350–361.
- Thomson, D.J., 1982. Spectrum estimation and harmonic analysis. *Proc. IEEE* 70 (9), 1055–1096.
- Wang, X.F., Metcalfe, I., Jian, P., He, L., Wang, C., 2000. The Jinshajiang–Ailaoshan suture zone, China: tectonostratigraphy, age and evolution. *J. Asian Earth Sci.* 18 (6), 675–690.
- Wang, X.F., Bachmann, G.H., Haggdorn, H., Sander, P.M., Cuny, G., Chen, X.H., Wang, C.S., Chen, L.D., Chen, L., Meng, F.S., Xu, G.H., 2008. The Late Triassic black shales of the Guanling area, Guizhou Province, south-west China: a unique marine reptile and pelagic crinoid fossil Lagerstätte. *Palaeontology* 51 (1), 27–61.
- Wang, X.-F., Chen, X.-H., Cheng, L., Wang, C.-S., Bachmann, G.H., Sander, M., Haggdorn, H., 2009. Sedimentary and palaeoecological environments of the Guanling and related biotas. *Acta Palaeontol. Sin.* 48 (3), 509–526 (in Chinese with English abstract).
- Xu, G., Niu, Z., Chen, H., 2003. Triassic cephalopods from the Zhuganpo and Xiaowa Formations in Guanling, Guizhou, with a discussion on the age of the Guanling biota. *Reg. Geol. China* 22 (4), 254–265.
- Yang, S., Liu, J., Zhang, M., 1995. Conodonts from the “Falang Formation” of Southwestern Guizhou and their age. *J. Stratigr.* 19, 161–170.
- Yin, G., Zhou, X., Cao, Z., Yu, Y., Luo, Y., 2000. A preliminary study of the early Late Triassic marine reptiles from Guanling, Guizhou, China. *Geology, Geochemistry* 28, 1–23.
- Zhang, C., Ogg, J.G., 2003. An integrated paleomagnetic analysis program for stratigraphy labs and research projects. *Comput. Geosci.* 29 (5), 613–625.